8-2018

The Effects of Geometric and Stoichometric Change in Nanoparticles and Materials on Lattice Thermal Conductivity

W. Tanner Yorgason
Utah State University

THE EFFECTS OF GEOMETRIC AND STOICHOMETRIC CHANGE IN NANOPARTICLES AND MATERIALS ON LATTICE THERMAL CONDUCTIVITY

by

W. Tanner Yorgason

A thesis submitted in partial fulfillment
of the requirements for the degree

of

MASTER OF SCIENCE

in

Mechanical Engineering

Approved:

Nicholas Roberts, Ph.D. Major Professor	Ling Liu, Ph.D. Committee Member
JR Dennison, Ph.D. Committee Member	Mark R. McLellan, Ph.D. Vice President for Research and Dean of the School of Graduate Studies

UTAH STATE UNIVERSITY
Logan, Utah

2018

ABSTRACT

The Effects of Geometric and Stoichometric
Change in Nanoparticles and Materials
on Lattice Thermal Conductivity

by

W. Tanner Yorgason, Master of Science
Utah State University, 2018

Major Professor: Nicholas Roberts, Ph.D.
Department: Mechanical and Aerospace Engineering

Thermal transport properties are critical for applications ranging from thermal management to energy conversion. Passive thermal management has been an area of study for over a century and has only grown as technology has advanced because it requires no additional energy to remove heat. Changing the nanostructure of the materials involved in passive heat transfer methods, either by geometric changes or stoichiometric changes, can greatly improve the effectiveness of this heat transfer method. In order to explore this further, this work employs LAMMPS molecular dynamics (MD) simulation software to calculate the lattice thermal conductivity (λ_p) of a nanoparticle (NP) and material used in different passive heat transfer methods after either modifying their geometry or stoichiometry. The NPs this work will simulate are single-wall carbon nanotubes (SWCNTs), which have been well known for high λ_p, and their applications in improving thermal conductivity in matrix materials. The material this work will simulate is magnesium silicide (Mg_2Si), a thermoelectric material. Thermoelectric materials, in general, become more efficient in converting heat into electrical power as their λ_p decreases. λ_p will be calculated for SWCNTs of varying lengths, diameters, and at varying equilibration temperatures (T_{eq}). λ_p will

be calculated for samples of pure Mg_2Si and Mg_2Si with off-stoichiometry over a range of T_{eq} values. Two methods will be used to induce the off-stoichiometry: atomic silicon (Si) substitutionals, and Si NPs. A range of stoichiometric ratios will be applied to the material by both methods, and then λ_p will be calculated for each of these cases. This is done so as to observe which method of stoichiometric change, given the same stoichiometric ratio, decreases λ_p greater, and, therefore, causes Mg_2Si to be a better thermoelectric material. It is expected that increases in length will increase the λ_p of the SWCNT, while increases in diameter and T_{eq} will decrease λ_p. It is expected that increases in atomic percent (a/o) Si and T_{eq} will decrease λ_p regardless of the method of stoichiometric change, and that the Si NP method will decrease λ_p more than the atomic Si substitutional method.

(70 pages)

PUBLIC ABSTRACT

The Effects of Geometric and Stoichometric
Change in Nanoparticles and Materials
on Lattice Thermal Conductivity
W. Tanner Yorgason

Thermal transport properties are critical for applications ranging from thermal management to energy conversion. Passive thermal management has been an area of study for over a century and has only grown as technology has advanced because it requires no additional energy to remove heat. Changing the nanostructure of the materials involved in passive heat transfer methods, either by geometric changes or stoichiometric changes, can greatly improve the effectiveness of this heat transfer method. In order to explore this further, this work employs LAMMPS molecular dynamics (MD) simulation software to calculate the lattice thermal conductivity (λ_p) of a nanoparticle (NP) and material used in different passive heat transfer methods after either modifying their geometry or stoichiometry. The NPs this work will simulate are single-wall carbon nanotubes (SWCNTs), which have been well known for high λ_p, and their applications in improving thermal conductivity in matrix materials. The material this work will simulate is magnesium silicide (Mg_2Si), a thermoelectric material. Thermoelectric materials, in general, become more efficient in converting heat into electrical power as their λ_p decreases. λ_p will be calculated for SWCNTs of varying lengths, diameters, and at varying equilibration temperatures (T_{eq}). λ_p will be calculated for samples of pure Mg_2Si and Mg_2Si with off-stoichiometry over a range of T_{eq} values. Two methods will be used to induce the off-stoichiometry: atomic silicon (Si) substitutionals, and Si NPs. A range of stoichiometric ratios will be applied to the material by both methods, and then λ_p will be calculated for each of these cases. This is done so as to observe which method of stoichiometric change, given the same stoichiometric ratio,

decreases λ_p greater, and, therefore, causes Mg_2Si to be a better thermoelectric material. It is expected that increases in length will increase the λ_p of the SWCNT, while increases in diameter and T_{eq} will decrease λ_p. It is expected that increases in atomic percent (a/o) Si and T_{eq} will decrease λ_p regardless of the method of stoichiometric change, and that the Si NP method will decrease λ_p more than the atomic Si substitutional method.

To Mom and Dad who told me to go back to school and do engineering.

ACKNOWLEDGMENTS

I would like to thank my Father in Heaven for guiding me down this path, my parents who told me to go back to school to do engineering (because they knew I was, and still am, a nerd), Dr. Roberts for all of his help, encouragement, and patience, the Utah Energy Research Triangle Program from the Governor's Office of Energy Development for providing the funding for this work, the Nuclear Regulatory Commission for providing additional funding for this work, the University of Utah CHPC for allowing USU to purchase and use their high computing resources, Dr. ChangJin Choi for his help and allowing me to gain experience, the NRC for providing funding for me throughout my entire time as a graduate student, Dr. Dennison for his help in Solid State Physics and agreeing to be on my committee, Dr. Liu for agreeing to be on my committee, Dr. Ebonee Walker who allowed us to use the script that got me started using LAMMPS, and all who helped me at various times in the lab, and in general in during this time in my life.

W. Tanner Yorgason

CONTENTS

Page

LIST OF TABLES

LIST OF FIGURES

CHAPTER 1

INTRODUCTION

Any device that uses or produces electrical or mechanical energy also uses or produces, to some extent, thermal energy. For this reason, thermal management has been an area of study for over a century and has only grown as technology has advanced. Appropriate thermal management can be achieved in a variety of ways, two of which are passive and active. Passive methods require no additional energy to move heat, and are therefore often favorable, though not always as effective as active methods. However, changing the nanostructure of the materials involved in passive heat transfer methods using nanoparticles (NPs) can have great effects on the thermal transport properties of these materials. This can, in turn, allow passive methods to become more effective, allowing improvements to passive methods such as greater efficiency in cooling systems for electronics, and greater waste heat recovery at power generation facilities.

One of the two efforts in this work was understanding the thermal conductivity (λ) of single wall carbon nanotubes (SWCNT), as they could significantly increase the λ of materials if the NPs are introduced into the materials matrix. This could increase the efficiency of current passive thermal management methods used in electronics. The second effort of this work was decreasing the λ of magnesium silicide (Mg_2Si) through addition of Silicon (Si) NPs, in order to improve its thermoelectric properties. This would allow more efficient conversion of heat into electricity, which would reduce the amount of heat lost to the environment in power plants, and maybe even vehicles.

1.1 Molecular Dynamics Simulations

Molecular dynamics (MD) simulations have been used for research for many years now, allowing researchers in various fields to simulate nanoscale and microscale material samples. Using periodic boundaries for the simulated space, or box, in which the material

is encased can allow for fairly accurate calculations of bulk material properties. Since the software to run these simulations is generally free under a General Public License (GPL), one obvious advantage of computational simulations over experimental work is monetary cost and time. Another advantage is the freedom in designing the material; perfect crystal lattices, placement of structures and particles with picometer accuracy, and changing the definition of potential energy between any number of particles are all possible. However, due to the complicated calculations that allow the simulations to imitate a physical experiment, the computational expense (the processing power a certain simulation requires to run within a given time) these simulations require can be high for computational work. Also, if the mathematical models for the interatomic potentials are not accurate, the results will be incorrect. The first problem can be mitigated through the use of periodic boundaries, parallelization of MD code, and knowing the minimum system size to represent bulk material properties. However, the challenge regarding interatomic potential equation accuracy is always a concern. Computational results are therefore verified by comparison against available experimental results.

The most commonly used MD software package is LAMMPS (Large-scale Atomic/Molecular Massively Parallel Simulator) and was originally developed in 1995 by Steve Plimpton [1]. Using LAMMPS, the λ of many materials has been determined, using a variety of methods. These calculations have been comparable to experimental results, which, combined with having the aforementioned advantage in freedom of simulating many different materials and structures, has made computational research using LAMMPS in material science and nanoscale heat transfer all the more popular.

There are, however, limitations in the calculation of λ using LAMMPS, one of which being that LAMMPS does not account for electrons in the simulations the software performs. This is significant, in view of Eqn. 1.1 [2]:

$$\lambda = \lambda_p + \lambda_e \tag{1.1}$$

where λ_p is the component of λ that comes from the atomic lattice vibrations (phonons)

in the material (known as lattice thermal conductivity), and λ_e is the component of λ that comes from the motion of electrons in a material. Since LAMMPS treats atoms in its simulations as spheres with no electrons, the λ_e component of λ in a given simulated material is always missing. This issue can be mitigated, however, by making use of certain add-on software available to LAMMPS, or simply by using materials with a negligible value of λ_e.

Many methods for calculating λ_p involve at least one equilibration ensemble, either before or during the phase of the simulation in which information from the system is recorded to calculate λ_p. The equilibration ensembles commonly used in such methods are the NPT, NVT, and NVE equilibration ensembles. The first two ensembles, NPT and NVT, time integrate the Nose-Hoover style non-Hamiltonian equations of motion, so as to match the positions and velocities of atoms sampled from the isothermal-isobaric (NPT) and canonical (NVT) ensembles, respectively. These, like most LAMMPS ensembles, only perform this integration on those atoms in the section of material the ensembles are applied to [1]. In both of these ensembles, the number of atoms is held constant and both target a constant temperature that can be input. The difference is that NPT targets a constant pressure that can be adjusted, while NVT targets a constant volume based on the initial volume when the ensemble begins. The NVE ensemble updates the positions and velocities of the atoms in the section of material it is applied to, but in a way that is consistent with the microcanonical ensemble [1]. Therefore, the NVE ensemble targets constant values for the number of atoms, the volume they occupy, and their total energy, based on these values when the NVE ensemble begins.

There are several methods which employ LAMMPS to calculate λ_p. Four of these methods are described below, along with their advantages and disadvantages. As one might assume, each method has different strengths and weaknesses, and so, each method is best suited for the simulation of different experimental setups. A summary of their advantages and disadvantages, along with experimental setups best suited for simulation by the method can be seen in Table 1.1.

1.2 Equilibrium Molecular Dynamics with Green Kubo Formalism

The equilibrium molecular dynamics (EMD) method assumes that the system is already in equilibrium, or close enough to it, that little if any equilibration is needed before data are collected from the system. For this reason, only the NPT or NVT ensembles are applied, sometimes in succession, beginning with the NPT ensemble. This method calculates λ_p without applying a heat flux or temperature gradient to the system. Instead, the energy and displacement of each atom are recorded during either the NPT or NVT ensemble (whichever one is applied last), and are used to calculate $\boldsymbol{J}$, using Eqn. 1.2:

$$\boldsymbol{J} = \frac{d}{dt}\sum_i E_i \boldsymbol{r}_i \tag{1.2}$$

where E_i is the energy per atom and $\boldsymbol{r}_i$ is the displacement of per atom with respect to the specific direction. $\boldsymbol{J}$ is in turn used to calculate $\boldsymbol{\lambda_p}$ using Eqn. 1.3, the Green Kubo formalism:

$$\boldsymbol{\lambda_p} = \frac{1}{3k_B T_{eq}^2 V}\int_0^\infty \langle \boldsymbol{J}(t)\boldsymbol{J}(0)\rangle dt \tag{1.3}$$

where k_B is Boltzmann's constant, T_{eq} is the equilibration temperature of the system, V is the volume of the system, and t is time. The factor of three in the denominator accounts for an average over three orthogonal directions in which λ_p is calculated. For a specific direction, this becomes Eqn. 1.4:

$$\lambda_{p\beta} = \frac{1}{k_B T^2 V}\int_0^\infty \langle J_\beta(t) J_\beta(0)\rangle dt \tag{1.4}$$

where β is the specific direction and J_β is a component of $\boldsymbol{J}$ in the specific direction. The calculation of $\boldsymbol{J}$, on through the calculation of λ_p, can be coded into the LAMMPS script or accomplished by an outside code after the simulation has run.

One of the biggest advantages of the EMD method is that it is computationally inexpensive. This is because it requires a relatively small number of atoms (on the order of 1000). This advantage also stems from the lack of an applied a heat flux, temperature

gradient, or any other non-equilibrium condition on the system. As non-equilibrium conditions such as these would increase the time needed for the system to reach equilibrium, their absence allows for the accumulation of valuable equilibrium state data in shorter time. Another advantage is the method's ability to allow periodic boundaries in all directions. This allows a λ_p calculation to take into account the longer phonon wavelengths that often contribute significantly to λ_p [3], as opposed to methods like the NEMD approach which are unable to account for these phonons without significant increase in computational cost, due to their non-periodic boundaries in at least one direction.

While the EMD method is much less computationally intensive than other MD methods, the post processing can be much more computationally expensive than that of other MD methods. This method is also limited in its ability to simulate more complicated geometries (such as large, non-crystalline systems), as it is usually only applied to cubic simulation boxes [3], [4], [5]. This would mean that a geometry with a significant length in only one direction would require, instead of just a rectangular prism to contain the geometry, a cube with a much greater volume. Thus the much greater volume translates to many more particles involved in the simulation, and so results in a greater computational expense. Finally, the EMD method can struggle with calculating accurate λ_p for materials with high λ_p [3]. This is because the time it can take for phonons in high λ_p materials to decay can be very long. Therefore, if the simulation is not run for a period of time that would allow all the phonons of a given material to decay naturally, the total energy the phonons carry in reality will be truncated, resulting in an undercalculation of λ_p [3].

1.3 Phonon Wave Packet

The phonon wave packet method, as described by Choi et al [6], allows for a direct observation of the behavior of phonons scattering at an interface during molecular dynamics simulations. This allows for calculation of α, the phonon energy transmission ratio, described by Eqn. 1.5:

$$\alpha = \frac{E_{tr}}{E} \tag{1.5}$$

where E_{tr} is the energy transmitted across the boundary, and E is the initial wave-packet energy.

In the PWP method, wave-packets are constructed from a single branch of the materials phonon dispersion curve, having a narrow frequency range, ω, and a well-defined polarization. The wave-packet is generated by displacing the materials atoms according to Eqn. 1.6:

$$u_n = A\epsilon \exp[ik(x_n - x_o) - (x_n - x_o)^2 \xi^{-2}] \tag{1.6}$$

where u_n is the displacement of the n^{th} atom, A is the amplitude of the displacement, ϵ is the polarization vector, k is the wave vector, x_n is the location of the atom along the direction of transport, x_o is the location of the center of the wave-packet, and ξ is the width of the wave-packet. Once formed, the wave-packet can be allowed to propagate through the material. As it encounters changes in the materials crystalline structure, it will either transmit, reflect, or partially reflect and transmit. This is accomplished through an MD simulation in which u_n is allowed to propagate through the system and across the boundary at an equilibration temperature (T_{eq}) of 0 K by means of an NVE ensemble [6]. For further accuracy, this step may be preceded by an MD equilibration run of the system, involving NPT, NVT, and NVE, usually applied in that order. In either case, once accomplished, α can be calculated using Eqn. 1.5. α can then be used to better understand energy transfer at the interface of the boundaries for a specific ω.

When α is calculated over a sufficient range of ω, such that α can be modeled as a function of ω, λ_p can be calculated by the Eqn. 1.7 (adapted from Gu et al [7]):

$$\lambda_p = \frac{L}{2\pi A^2} \int_0^\infty \hbar\omega \frac{\partial n^0(\omega, T_{eq})}{\partial T_{eq}} Tr(\omega) DOS(\omega) d\omega \tag{1.7}$$

where L is the length of the sample in the direction of the heat flux, A is the cross-section

area perpendicular to the direction of the heat flux, $\hbar$ is Planck's constant divided by 2π, ω is the frequency of a given phonon, n^0 is the equilibrium phonon distribution function, $Tr(\omega)$ is the transmission coefficient, α, at a given ω, and $DOS(\omega)$ is the phonon density of states at a given ω.

The PWP method is particularly useful for boundary conductance and resistance, the boundary being a change in the systems crystalline structure, material, or both. This method is useful because other simulation methods would be more computationally intensive and cannot easily, if at all, recover the information necessary to calculate α. The higher computational expense comes from the fact that the other methods require a larger number of atoms or require more intensive post processing. The higher T_{eq} the other methods often employ introduces more phonons, and phonons in practically random directions, to the system, making the recovery of information regarding the energy loss of a phonon as it passed through an interface difficult at best. Further, since the PWP method uses only a single branch of the materials phonon dispersion curve, with a narrow frequency range, and a well-defined polarization, it is much easier to track how much of this wave is transmitted to the other side of the boundary, as it can practically be treated as a phonon.

For this same reason, the PWP method is not advantageous when simulating systems for bulk λ_p. This is because in simulating only a single branch of the materials phonon dispersion curve, with a narrow frequency range, and a well-defined polarization, only a very small portion of the materials total heat transfer processes can be represented, resulting in an underestimation of λ_p. Worse still, this underestimation can be anywhere from slight to drastic, since the information given is used to describe the heat transfer processes of essentially only one phonon.

1.4 Non-equilibrium Molecular Dynamics

Another method for calculating λ_p is the non-equilibrium molecular dynamics (NEMD) method. This method builds on the EMD method in that it also applies the NPT and NVT ensembles. This method differs, however, in that it applies a third ensemble to equilibrate the system, namely, the NVE ensemble. This additional equilibration ensemble is added

so that the system can further equilibrate, in hopes of further accuracy in the results of the simulation. The other exception is that a non-equilibrium condition is applied to the system during the NVE ensemble, such as a heat flux or temperature gradient. This condition is usually applied after the NVE ensemble has run for some time, allowing for proper equilibration of the system before the non-equilibrium condition is applied.

After the non-equilibrium condition has been employed and the system has reached a steady state, information from the system is collected. Information regarding the non-equilibrium method used (for example, the value of the applied heat flux) is used with the system's collected information (for example, the temperature gradient) to calculate λ_p. As λ_p usually only applies to solids, it is calculated using Eqn. 1.8, Fourier's law:

$$q = -\lambda_p \frac{dT}{dx} A \tag{1.8}$$

where q is the energy added and subtracted from the system per timestep (so as to apply a heat flux), A is the area that q is passing through, and $\frac{dT}{dx}$ is the temperature gradient. Rearranging Eqn. 1.8, Eqn. 1.9 is obtained:

$$\lambda_p = -\frac{q}{A} \frac{dx}{dT} \tag{1.9}$$

which can be used to calculate λ_p.

The NEMD method is advantageous for systems with complicated geometries, as the system size is generally required to be large in order to ensure the longer phonon modes are accounted for. These systems can also take on almost any shape, though it is often preferred that it be a rectangular prism, the longer dimension being parallel with the heat flux or temperature gradient. This advantage is the most critical, as it enables exact control over atomic placement in systems of at least 100,000 atoms. The NEMD method thus allows one to create virtually any nanoscale solid-state structure and retrieve simulated values for λ_p or other material properties. Another advantage of the NEMD method is its relatively simple post processing requirements as compared to EMD, PWP, and other MD methods.

Simply put, the NEMD method does most of the computational work upfront, whereas the other methods do less, and so need more post processing work than the NEMD method. Finally, this method often results in a better approximation of a real system, as it involves 100,000 or more atoms.

The biggest disadvantage of the NEMD method is the computational expense. In MD simulations, computational expense scales with N^3, N being the number of particles within the simulation. Also, NEMD simulations are required to be longer in the direction of the heat flux or temperature gradient so as to better capture all possible phonon modes in the material. These facts, combined with the fact that NEMD simulations need to simulate a longer time period (often 15 nanoseconds (ns)) of real time, ensure that NEMD simulations have much greater computational cost than other comparable methods. In addition, care must be used to ensure that the temperature gradient information used is along the linear portion of the curve, far enough away from both the heat source and sink where the flux is being added and subtracted. In order to retrieve the information required to calculate λ_p, post processing scripts may be necessary as the time that these simulations need to be run, and the rate of output, produces large text files (100 Mb or more).

1.5 Normal Mode Decomposition

A more recent method of calculating λ_p is normal mode decomposition (NMD). This method was developed by Alan McGaughey, and uses the EMD method with the Green Kubo formalism. The difference is that this method divides up the phonons in groups based on their frequencies in order to get λ_p values for each phonon frequency group.

The actual application of this method is very complex, and so the process for the NMD method will largely be summarized by the following adaptation from McGaughey et al [8]. After a material and its atomic structure are selected, a unit cell needs to be chosen. The cell will be the entire physical space that LAMMPS will simulate, and so can be thought of as the simulation cell. Next, the allowed wave vectors are specified for the simulation cell. Once specified, quasi-harmonic lattice dynamics calculations are performed in order to obtain the frequencies and mode shapes of all normal modes associated with this material

and its atomic structure. MD simulations are then run so that the position and velocity of each atom is output. Finally, the atomic positions and velocities are projected onto the normal mode coordinates. For a time-domain or frequency-domain analysis, the reader is referred to [8], as a more in-depth explanation can be found in the original work.

Because this information allows one to identify the λ_p dependencies for certain ranges of phonon modes, one can then better know which ranges of modes are most important to λ_p, and which are not. These more important ranges of phonon modes can then be targeted as what should be preserved, as opposed to the entire spectrum of phonons, if the material undergoes changes in crystalline structure or stoichiometry. This also has applications in heat transfer between two, or more, materials. For example, instead of looking at the available phonon modes of each material, and trying to match every, or even most, phonon modes, one could simply focus on finding a match between the ranges of modes that contribute most to each materials λ_p, all but eliminating thermal boundary resistance.

The biggest advantage of this method is the information that it makes available about the material. The previous paragraph gives one example of an application of this information, however there are many others, such as mismatching the contributing ranges of phonon modes purposefully so that better insulation is obtained. One advantage that results of all the information made available is a more accurate calculation of λ_p. An example of this can be seen in [9] and [4].

The biggest disadvantage of the NMD method is the post processing computational expense. The simulations are essentially EMD simulations, and so run fairly quickly, but the post processing for NMD is considerably more involved than the EMD, as can be seen early in this section. The NMD method also requires extra software, such as GULP, to generate a phonon dispersion relation, and obtain normal mode information used in the NMD process. Other disadvantages are those seen in the EMD method, such as struggling with simulating large, non-crystalline systems and materials with high λ_p.

Table 1.1: Advantages and Disadvantages of Various MD Methods for Calculation of λ_p

MD Method	**Advantages**	**Disadvantages**
EMD	• Computationally inexpensive • Can give more accurate λ_p • Does not require an applied heat flux or temperature gradient • *Ideal for*: λ_p calculation of single crystalline materials	• Cannot represent asymmetric geometry • Computationally expensive post-processing requirements Struggles with calculating materials with high λ_p
PWP	• Computationally inexpensive • Gives more detailed information regarding a specific range of phonon frequencies • *Ideal for*: λ_p calculation across material or crystalline boundaries	• Only gives information for a specific range of phonon frequencies • Cannot easily account for effects of complex stoichiometric changes on λ_p
NEMD	• Handles complex lattice geometries such as NPs, defects, and stoichiometric changes well • Post processing is computationally inexpensive • Uses a larger number of particles (˜100,000) and simulates a longer period of time (often 15 ns), thus better simulating a real system • *Ideal for*: λ_p calculation materials with complex and/or stoichiometry or unique crystalline structure	• Computationally expensive • Simulations need to be long in the direction of the heat flux to produce accurate results for λ_p • Needs to simulate a longer period of time (often 15 ns) of real time to be valid
NMD	• Shows the contribution of phonon normal modes to λ_p • More accurately calculates λ_p • *Ideal for*: Very accurate λ_p calculation of single crystalline materials	• Post processing is very computationally expensive • Struggles to simulate large non-crystalline systems • Requires use of lattice dynamics program, such as GULP, to generate a phonon dispersion relation, and obtain normal mode information

1.6 The Method Chosen for This Work: NEMD

The NEMD method was chosen for this work for a variety of reasons. First, and most importantly, it allows much more complicated geometries in the system, geometries for which none of the other methods can accurately calculate λ_p. This fact makes the NEMD method ideal for changing the nanostructure of the system, especially along a particular direction or directions. This is important for simulating anisotropic changes in the nanostructure of materials, such as changing the diameter and length of a SWCNT or adding Si NPs to the lattice of Mg_2Si. Because total differences in computational time plus post processing time for each method are roughly equivalent, this is the most important reason for choosing the NEMD method. However, other reasons are given in the following two paragraphs.

Also, the NEMD method can calculate an accurate λ_p for SWCNTs, which NPs have a notoriously high λ_p (see Table 1.2), unlike the EMD method. In addition, because the NEMD method uses a larger number of particles and simulates a longer time period, it can be seen as a more accurate method for calculating λ_p for materials that have had mixed results for λ_p in the past. SWCNTs are NPs that clearly fall into this category, as can be seen in Table 1.2. Further, though the λ_p of Mg_2Si has been known for some time [10], changes to λ_p made by stoichiometric change to the material are not nearly as well established. Therefore, the NEMD method should help to better approximate correct values for λ_p for these materials.

Another reason for choosing the NEMD method is for ease of post processing. For Mg_2Si and SWCNTs, determining and correcting errors in λ_p calculation using an EMD or NMD approach can be difficult due to the complicated nature of the post processing calculations. The NEMD method post processing, however, is not only less computationally expensive, but also involves simpler calculations, and therefore results in post processing code that is easier to debug. As an example, a script of some kind, if not a very complex one, is needed to compute λ_p for the other methods, where, depending on length of time run and frequency of data taken, the post processing for the NEMD method can be computed using a Microsoft Excel spreadsheet. This simple nature of the post processing for the NEMD

method also eases the work of determining whether the source of the erroneous λ_p is in the LAMMPS script or post processing method. More information regarding the advantages of this method can be seen in Table 1.1.

The remainder of this document will consist of the Objectives, Approach, Nanoparticle and Material Backgrounds, Simulations Setup, Results and Discussion, Conclusion, and References chapters. The Objectives chapter consists of the list of objectives this work intends to fulfill. The Approach chapter consists of the plan to meet the aforementioned objectives. The Nanoparticle and Material Backgrounds chapter covers some information about the materials and the reason for the investigation of their respective λ_p values. The Simulations Setup chapter explains the setup details for the LAMMPS simulation. The Results and Discussion chapter consists of the presentation of the results, and their associated potential explanations. The Conclusion chapter contains specific conclusions for SWCNT and Mg_2Si, and a general conclusion based on both works. Lastly, the References chapter consists of a list of sources cited by this work.

Table 1.2: λ_p of isolated SWCNT at T_{eq} of 300 K* obtained using computational and experimental techniques and some setup information (adapted from Lukes et al [11])

Molecular Dynamics Simulations					
Reference	λ_p ($Wm^{-1}K^{-1}$)	SWCNT Length (nm)	Cross-Sectional Area (m^2)	Chirality	Simulation Technique
Osman et al. [12]	1700	30	14.6×10^{-19}	(10, 10)	NEMD
Che et al. [13]	2980	40	4.3×10^{-19}	(10, 10)	EMD
Yao et al. [14]	1 - 4×10^{23}	6 - 60	14.6×10^{-19}	(10, 10)	EMD
Padgett and Brenner et al. [15]	40 - 320	20 - 310	14.6×10^{-19}	(10, 10)	NEMD
Moreland et al. [16]	215 - 831	50 - 1000	14.6×10^{-19}	(10, 10)	NEMD
Maruyama et al. [17]	260 - 400	10 - 100	14.6×10^{-19}	(10, 10)	NEMD
Boltzmann-Peierls Phonon Transport Equation (*T_{eq} = 316 K)					
Reference	λ_p ($Wm^{-1}K^{-1}$)	SWCNT Length (nm)	Cross-Sectional Area (m^2)	Chirality	Simulation Technique
Mingo and Broido [18]	80 - 9500	10 - 10^9		(10, 10)	
Experimental Measurement					
Reference	λ_p ($Wm^{-1}K^{-1}$)	SWCNT Length (nm)	Diameter (nm)		
Yu et al. [19]	2000	2600	1		
Yu et al. [19]	1×10^4	2600	3		
Pop et al. [20]	3400	2600	1.7		

CHAPTER 2

OBJECTIVES

1. Using LAMMPS MD software and applying the NEMD method, obtain values for λ_p of SWCNT at various T_{eq} (50 to 500 K, at 50 K increments), lengths (25, 100, and 200 nm), and diameters (1.5 and 6.9 nm)

2. Using LAMMPS MD software and applying the NEMD method, obtain values for λ_p of Mg_2Si at various stoichiometries modified by number of Si NPs (0, 1, 2, 4, 8, and 16 NPs) and at various T_{eq} (300, 600, and 900 K)

3. Using LAMMPS MD software and applying the NEMD method, obtain values for λ_p of Mg_2Si at various stoichiometries (those corresponding to the stoichiometries generated in objective 2) modified by substitutional Si atoms (33.33, 34.29, 35.32, 37.29, 41.37, and 49.55 a/o Si) and at various T_{eq} (300, 600, and 900 K)

CHAPTER 3
APPROACH

3.1 SWCNT

The following will be done on my personal computer and a research desktop in ENLAB 205. First, a method to create the lattice structure of the SWCNTs to be simulated will be developed. Then, the consistent valence force field (CVFF) potential, as used in Zang et al [21], will be implemented to describe the interatomic potential of the carbon atoms in the SWCNT. The Visual Molecular Dynamics (VMD) software [22] will be used to build the crystal structure (in this case, perfect crystalline structure) of each of the SWCNTs. Each simulation will be run for a total of 2 ns, using a timestep of 1 fs, and an equilibration process consisting of the NPT, NVT, and NVE ensembles. Next, using this lattice structure and potential model, a reasonably accurate λ_p for a given SWCNT will be obtained. Following these initial steps, changes in length, diameter, and T_{eq} will be made to the original SWCNT, according to what is stated in the Objectives chapter, and λ_p will be calculated for each new system created by these changes, so that the effects of each change on λ_p can be calculated. The results will then be plotted as λ_p vs. SWCNT T_{eq} graphs; one graph displaying information regarding changes in SWCNT length, the other displaying information regarding changes in SWCNT diameter.

3.2 Mg_2Si

The following will be done on my personal computer, a research desktop in ENLAB 205, and using the Center for High Powered Computing (CHPC) at the University of Utah. First, a method to create the lattice structure of Mg_2Si will be developed, so as to create the perfect crystalline antifluorite lattice of Mg_2Si. A method will also be developed to create the perfect crystalline diamond lattice of the pure Si NPs. Then, an extended MEAM potential

developed by Zhang et al [23] will be implemented to describe the interatomic potential of Mg_2Si, pure Si (for the Si NPs), and off-stoichiometry Mg_2Si. Each simulation will be run for a total of 15 ns, using a timestep of 1 or 0.1 fs (depending on the level of complexity of the stoichiometry and lattice structure), and an equilibration process consisting of the NPT, NVT, and NVE ensembles. Using these lattice structures and potential model, a reasonably accurate λ_p for bulk Mg_2Si will then be obtained. Following these initial steps, changes in stoichiometry, both by addition of Si NPs (achieved through the LAMMPS MD software) and addition of substitutional Si atoms (achieved using a MATLAB script), will be implemented. The Si atomic percent (a/o) and T_{eq} of the systems will then be changed, the first being modified either by addition of Si NPs or substitutional Si atoms. These changes will be made according to what is stated in the Objecives chapter. As a reference system, a pure Mg_2Si system will undergo the same changes as the stoichiometrically modified systems, with the exception of the changes in stoichiometry; i.e., only T_{eq} will be changed. For each change to each system, λ_p will be calculated so as to quantify the effect of each of the aforementioned system modifications on λ_p. This information will then be plotted so that there are four graphs total: λ_p vs. T_{eq} and λ_p vs. Si a/o for stoichiometric manipulation Mg_2Si by substitutional Si, and λ_p vs. T_{eq} and λ_p vs. Number of Si NPs Present in Mg_2Si for stoichiometric manipulation Mg_2Si by addition of Si NPs. Each of the λ_p vs. T_{eq} graphs will include the plot of information for the pure Mg_2Si whose only modifications were in T_{eq}.

CHAPTER 4

Nanoparticle and Material Backgrounds

4.1 SWCNT

SWCNT have long since been known for their high λ_p, and so much work has been done to use these NPs to enhance the λ_p of other materials by embedding SWCNTs in said materials. One of the most prominent examples of this is embedding SWCNTs in polymers to improve the λ_p of the composite material. A composite polymer with a high λ_p would have important applications in heat exchangers, computer components, and other thermal devices where an electrically insulative but thermally conductive material is desired. Ideally, the composite would also be lightweight, flexible, corrosion resistant, and relatively easy to process [24].

Information critical to the results of these efforts is the λ_p of the SWCNTs themselves, which can depend on a variety of factors such as T_{eq}, length [3], diameter [25], and others. Current SWCNT fabrication processes can manipulate the length of the NPs and perhaps even the diameters of the SWCNTs [26]. This work seeks to understand how the λ_p of SWCNTs is affected by changes in these parameters. All of the systems generated by VMD [22] are perfect crystalline, in contrast to the reality of fabricated SWCNTs; however, general trends in changes in λ_p based on changes in length, diameter, T_{eq} should be valuable predicting changes in λ in real SWCNTs based on length, diameter, and actual T.

4.2 Mg_2Si

4.2.1 Note

This and all sections following regarding Magnesium Silicide (Mg_2Si) are taken from a journal article [27] written by the author, which was published in MRS Advances in August of 2017. Information from the journal article is included here for purposes of completeness.

Addition of Si NPs to Magnesium Silicide (Mg_2Si), a well-known thermoelectric, may increase this materials efficiency in waste-heat recovery, as shown in similar work [28]. The figure of merit (ZT), which is used to determine the efficiency of a thermoelectric material to convert heat into electric power, is a dimensionless parameter described by Eqn. 4.1 [2]:

$$ZT = S^2 \frac{\sigma T_{abs}}{\lambda} \tag{4.1}$$

where S is the Seebeck coefficient, σ is the electrical conductivity, T_{abs} is the absolute temperature, and λ is the thermal conductivity of the thermoelectric material. Eqn. 4.1 shows that ZT can be increased by lowering the λ of the material. λ is defined by equation Eqn. 1.1 in the introduction.

Usually, the positive correlation between λ and σ, which occurs due to the positive correlation between λ_e and σ, presents a challenge in achieving a high ZT value in thermoelectric materials. However, at 300 K, the λ_e of Mg_2Si is very small relative to λ, being 0.2 $Wm^{-1}K^{-1}$ or less [29], while λ has been measured at 7.8 $Wm^{-1}K^{-1}$ [10]. Therefore, λ should depend much more on changes in λ_p than changes in λ_e. Further, the Si NPs (32.562 Å in diameter) should cause much more phonon scattering than electron scattering, due to the size difference in the mean free paths of phonons and electrons [30]. Therefore, the presence of Si NPs should not cause a significant change in σ or λ_e . In addition, adding Si NPs to a material is known to increase S [31].

From [32], Mg_2Si is not magnetic, and its magnetic properties should not be affected by the proposed stoichiometric changes. This implies that thermal properties of this material and those of its stoichiometrically changed systems should not be affected by their magnetic properties, as these properties would be and remain nonmagnetic. Given this information, decreasing λ_p using Si NPs should result in a higher ZT value. Though decreasing λ_p through the addition of Si NPs should increase ZT, LAMMPS [1], the MD software used, can only calculate λ_p, as mentioned in the introduction. This fact necessitates further research to obtain the S, σ, and λ values for each of our systems in order to calculate accurate ZT values, and thus identify the nanostructure resulting in the greatest ZT value.

The focus of the work with Mg_2Si, therefore, is to find the nanostructure resulting in the lowest λ_p value, so as to provide a strong starting point for these future efforts.

CHAPTER 5

Simulations Setup

5.1 SWCNT

As mentioned in the introduction, the NEMD equilibration process was used in conjunction with LAMMPS [1] MD software. VMD software [22] was used to create data files to define the positions of each atom, their bonds, bond angles, dihedrals, and impropers in the SWCNTs. Data files for SWCNTs of lengths of 25, 100, and 200 nm, each with a diameter of 1.5 nm, were created using VMD. One last data file was created for a SWCNT with a length of 200 nm and a diameter of 6.9 nm to compare the diameter differences. For simplicity purposes, the diameter of any SWCNT mentioned hereafter will be 1.5 nm unless otherwise stated. Due to inexperience at the time this work was done, and that diameters were could only be controlled indirectly, these two diameters alone were applied to the SWCNTs. These data files were then read by LAMMPS input files, one for each of the data files generated. See Figure 5.1 for a visual representation of the SWCNTs generated using VMD.

Each LAMMPS [1] input file was written so that it constructed a unit cell simulation box (see Figure 5.2), with dimensions oriented along the x-, y-, and z-axes, respectively (the longest dimension being along the z-axis). The boundaries of the simulation box were set to be periodic, but sufficient space was placed between the boundaries in the x- and y-directions and the SWCNT to ensure that the simulation calculated λ_p for only one SWCNT, not many right next to one another. SWCNT hot and SWCNT cold sections of the material were created close to either end of the simulation box, which act as a heat source and a heat sink, creating a constant heat flux. To ensure that these sections would not interfere with each other due to the nature of the periodic boundaries, both ends of the simulation box were capped with SWCNT walls, or sections of the material in which the atoms do not

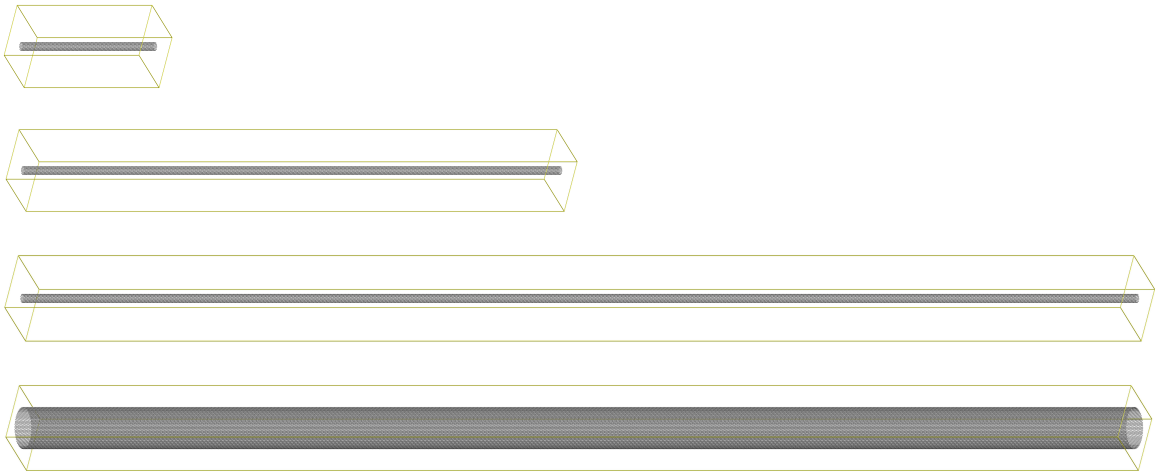

Fig. 5.1: Visual representation of the 25, 100, 200 nm, and 69 nm diameter, SWCNTs, from top to bottom, respectively. The yellow lines are the edges of the simulation box.

move. Here symmetry was not important since, due to the periodic boundaries, these two sections were in reality one section. The segment tested for λ_p was the material between the heat source and sink. For clarity purposes, this section, whose λ_p is measured, will be referred to as the SWCNT test section. A visual representation of the simulation setup can be seen in Figure 5.2.

As the length of the SWCNT changed, so did the simulation box length and the lengths of each section (SWCNT hot, cold, test, and wall sections) in the z-direction. For the 25 nm length SWCNT, the lower SWCNT wall section length was 20.6 Å, the SWCNT cold section length was 21 Å, the SWCNT test section length was 167 Å, the SWCNT hot section length was 21 Å, and the upper SWCNT wall section length was 20.9 Å, making a total length for the unit cell simulation box 250.5 Å. For the 100 nm length SWCNT, the lower SWCNT wall section length was 99.5 Å, the SWCNT cold section length was 101 Å, the SWCNT test section length was 600 Å, the SWCNT hot section length was 101 Å, and the upper SWCNT wall section length was 99.5 Å, making a total length for the unit cell simulation box 1001.0 Å. For the 200 nm length SWCNT, the lower SWCNT wall section length was 199.5 Å, the SWCNT cold section length was 201 Å, the SWCNT test section length was 1100 Å, the SWCNT SWCNT hot section length was 201 Å, and the upper SWCNT wall section length was 199 Å, making a total length for the unit cell simulation

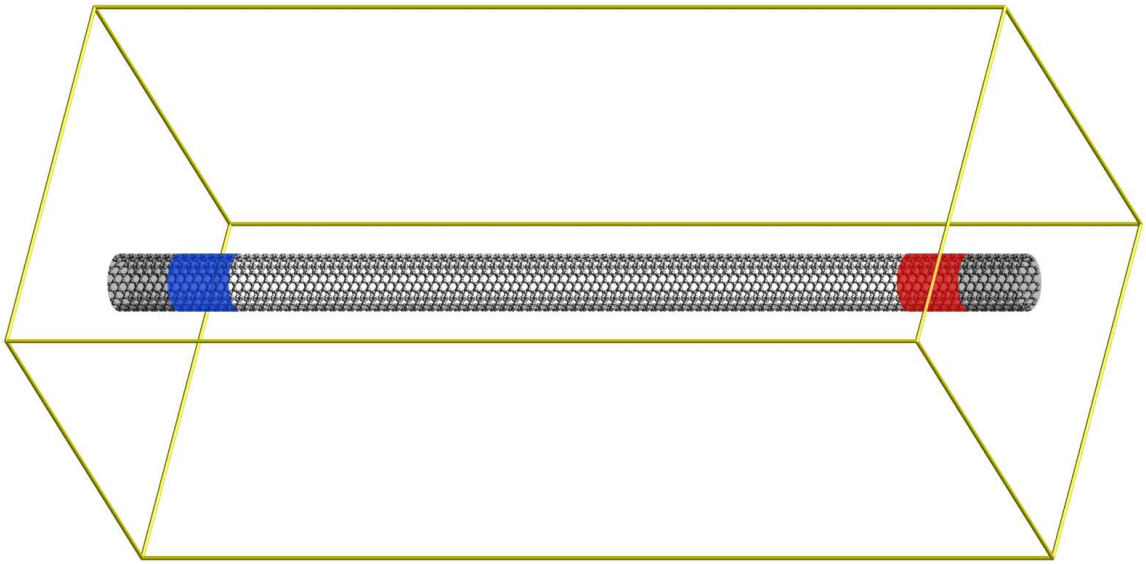

Fig. 5.2: Visual representation of the simulation setup using the 25 nm long SWCNT system as an example. The red-shaded volume represents the SWCNT hot section, the blue-shaded volume the SWCNT cold section, and the gray-shaded volumes represent the SWCNT wall sections. The yellow lines are the edges of the unit cell simulation box.

box 2000.6 Å. For all SWCNT systems, the dimensions in the x- and y-directions were 100 Å. These systems will continue to be referred to as the 25 nm, 100 nm, and 200 nm SWCNT systems, respectively, although their actual length differs slightly from these values. The dimensions used for the 200 nm SWCNT system were also used for the 69 nm diameter SWCNT system.

Because of the nature of the output of VMD, specifically its including information on bonds, bond angles, dihedrals, and impropers, a molecular style was used in conjunction with the atom_style command in the aforementioned LAMMPS input files. This style, along with the information provided by the VMD software, required that only certain interatomic potentials be employed. Specifically, the interatomic potentials were required to provide information regarding each bond, bond angle, dihedral, and improper, such as associated energy and angle values. The potential selected was the constant valence force field, as implemented by Zang et al [21]. Eqn. 5.1 through Eqn. 5.6 describe the potential in greater detail.

$$E = E_{pair} + E_{bond} + E_{angle} + E_{dihedral} + E_{improper} \tag{5.1}$$

where E is the total energy of the interatomic potential, and E_{pair}, E_{bond}, E_{angle}, $E_{dihedral}$, and $E_{improper}$ are defined by Eqn. 5.2 through Eqn. 5.6

$$E_{pair} = 4\epsilon_E \left[\left(\frac{\sigma_r}{r} \right)^{12} - \left(\frac{\sigma_r}{r} \right)^{6} \right], r < r_c \tag{5.2}$$

where σ_r is the distance at which the interatomic potential is zero, ϵ_E is the depth of the interatomic potential well, r is the distance between one atom and another, and r_c is the cutoff distance, or the distance over which this potential equation is applied.

$$E_{bond} = K_b(r_b - r_{b0})^2 \tag{5.3}$$

where K_b is the stiffness of the bond, r_b is the bond length, and r_{b0} is the bond length reference value.

$$E_{angle} = K_a(theta - \theta_0)^2 \tag{5.4}$$

where K_a is the stiffness of the bond angle, and θ is the value for the bond angle, and θ_0 is the bond angle reference value.

$$E_{dihedral} = K_d[1 + d_d cos(n_d \psi_d)] \tag{5.5}$$

where K_d is the energy barrier height of the dihedral angle, d_d represents the direction of dihedral angle (having a value of either -1 or +1), n_d is the multiplicity of the dihedral angle, and ψ_d is the value for the dihedral angle.

$$E_{improper} = K_i[1 + d_i cos(n_i \psi_i)] \tag{5.6}$$

where, similar to Eqn. 5.5, K_i is the energy barrier height of the improper angle, d_i represents the direction of improper angle (having a value of either -1 or +1), n_d is the multiplicity of

the improper angle, and ψ_i is the value for the improper angle.

The necessary coefficients and constants, from [21], for the CVFF potential were then converted to the unit system used by the LAMMPS input file, and implemented in the input file. The coefficients and constant used in Eqn. 5.2 were not used, but instead other parameters (namely $\epsilon_E = 1$ eV, $\sigma_r = 1$ Å, and $r_c = 1$ Å) were used. The application of this potential and the aforementioned coefficients and constants led to stable systems from T_{eq} of 50 through 500 K. This system stability was taken to imply that this potential was valid for the SWCNT systems in this work.

Each simulation was run for a total of 2 ns to ensure that the systems reached steady state. This shorter run time was possible due to SWCNTs being thermally fast, resulting in thermal equilibration for the NP in less time than most materials. The 2 ns were divided so that most of the time was given to the constant heat flux application, as follows: NPT and NVT each ran for 0.3 ns, NVE ran for 0.4 ns, then NVE continued to run while a constant heat flux was applied for an additional 0.1 ns, and the remaining 0.9 ns were used to record temperature gradients every 0.2 ps, while the NVE and constant heat flux continued to run. Each of the systems were simulated at T_{eq} of 50, 100, 150, 200, 250, 300, 350, 400, 450, and 500 K, and at an equilibration pressure of 0.0 bars.

The temperature values composing the temperature gradient were collected in the following way. The temperature values were averaged both temporally and spatially, being determined by a time increment (0.2 ps) to be averaged over as well as a 3-dimensional space to be averaged over. The 3- dimensional space, or chunk is determined by a length value, which is used to break up the SWCNT test section into rectangular prisms along the z-direction, with divisions being perpendicular to the z-direction every certain chunk size length value. The chunk size values of 25, 100, and 200 Å were used in each simulation according to the length of the SWCNT simulated (25, 100, and 200 nm respectively). Using the aforementioned averaging process, the occurrence of steady state in these average temperature values was identified. The average temperature values were averaged over the time from the beginning of steady state until the end of the simulation. This process,

which was repeated for each system, provided a temperature gradient for the entire SWCNT test section. As mentioned in the introduction, Eqn. 1.9 was modified to account for the direction of the heat flux as shown in Eqn. 5.7:

$$\lambda_p = -\frac{q}{A}\frac{dz}{dT} \tag{5.7}$$

Eqn. 5.7 was then used to calculate the λ_p of each system. This equation was used over a number of chunks to obtain a more accurate temperature gradient, and thus a more accurate value for λ_p. The number of chunks used varied from 3 to 7, in an effort to ensure that Eqn. 1.9 was only applied over linear portions of the temperature gradient.

In calculating λ_p for SWCNTs, there are at least two ways calculate A. One is to calculate the circular area of the SWCNT ("circle method") and the other is to calculate only that area that is associated with the material itself, in other words, A is calculated as an annulus ("annulus method"). This work uses the latter method which, in view of Eqn. 1.9, leads to much higher values of λ_p. According to the annulus method used by this work, A scales with $d/2$, d being diameter. If the circle method is used instead, A scales with $d^2/4$. If one takes these different methods for calculating A into account, and adjusts accordingly, then the resulting trends in λ_p are the same, regardless of the choice between the two methods for calculating A. However, throughout this work with SWCNTs, unless otherwise mentioned, A will be calculated using the annulus method.

5.2 Mg_2Si

As mentioned in the introduction, the NEMD equilibration process was used with LAMMPS [1] MD software. This method of using the NPT, NVT, and then NVE ensembles is especially helpful when T_{eq} is 600 or 900 K. This is because these higher T_{eq} values are likely to cause thermal expansion, which longer equilibration processes should more accurately capture.

A LAMMPS input file was written so that it constructed an 8 by 8 by 128 unit cell (50.704 by 50.704 by 811.264 Å) simulation box (see Figure 5.3), with dimensions oriented

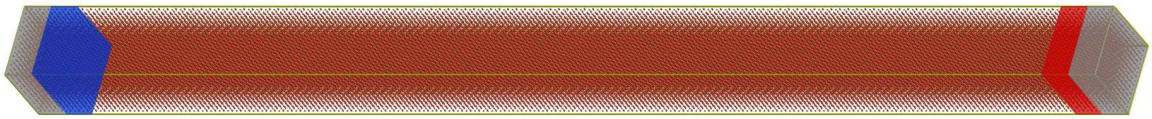

Fig. 5.3: Visual representation of the simulation setup using the pure Mg_2Si system as an example. The red-shaded volume represents the Mg_2Si hot section, the blue-shaded volume the Mg_2Si cold section, and the gray-shaded volumes represent the Mg_2Si wall sections.

along the x-, y-, and z-axes, respectively (the longest dimension being along the z-axis). The boundaries of the simulation box were set to be periodic so that bulk λ_p could be better simulated. Mg_2Si hot and Mg_2Si cold sections of the material were created close to either end of the simulation box, which act as a heat source and a heat sink, creating a constant heat flux. These Mg_2Si hot and Mg_2Si cold sections were each 47.535 Å in length in the z-direction. To ensure that these sections would not interfere with each other due to the nature of the periodic boundaries, both ends of the simulation box were capped with Mg_2Si walls, or sections of the material in which the atoms do not move. These Mg_2Si wall sections were 44.366 and 47.535 Å in length in the z-direction. Here symmetry was not important since, due to the periodic boundaries, these two sections were in reality one section. The segment tested for λ_p was the material between the heat source and sink, and though it varied slightly between systems due to the movement of atoms as the system equilibrated, this section was initially 624.293 Å in length in the z-direction and changed by no more than 50 Å. For clarity purposes, this section, whose λ_p is measured, will be referred to as the Mg_2Si test section. A visual representation of the simulation setup can be seen in Figure 5.3.

In order to initialize the locations of the Mg and Si atoms for the simulation, an antifluorite lattice structure consisting of an FCC lattice with a lattice constant (a) equal to 6.338 Å for the Si atoms, and a BCC lattice with a equal to 3.169 Å for the magnesium (Mg) atoms, was employed. Each Mg BCC lattice was centered within each Si FCC lattice. The Si NP system simulations used spherical pure Si NPs, all oriented in the center of the simulation box, parallel to the z-axis, and evenly spaced along this axis. A diamond lattice was used for the Si NPs, with an a of 5.427 Å. The diameter of each Si NP was 32.562 Å

(See Figure 5.4). In order to ensure that the stoichiometry of the substitutional Si atoms in the Mg_2Si matrix matched that of the Si NP systems, a MATLAB script was written to read in a LAMMPS data file for pure Mg_2Si, which contained the positions of every atom in the simulation box. It then identified the Mg atoms by their assigned type in the data file, which was 1, and randomly replaced them with 2, which was the type assigned to the Si atoms. This was done according to the target a/o Mg, which was entered at the beginning of the script. The target a/o Mg and the results differed by less than 1 a/o Mg (See Figure 5.4). The a/o targeted was that of each respective system involving Si NPs, so as determine whether the decrease in λ_p was caused by the nanostructure or by the stoichiometry of the systems of Mg_2Si with Si NPs. From This should have a similar effect as the NP addition to Mg_2Si [33], the Si atomic substitutions should have an effect similar to the NP addition to Mg_2Si on λ_p. These data files were then read in by a LAMMPS input script so that each Mg_2Si system could be simulated.

As a note for clarity: all systems, including the Si NPs, were single crystalline, the only defects being Si NPs, and substitutional Si atoms in the Mg_2Si matrix. For more detail, see Figure 5.4.

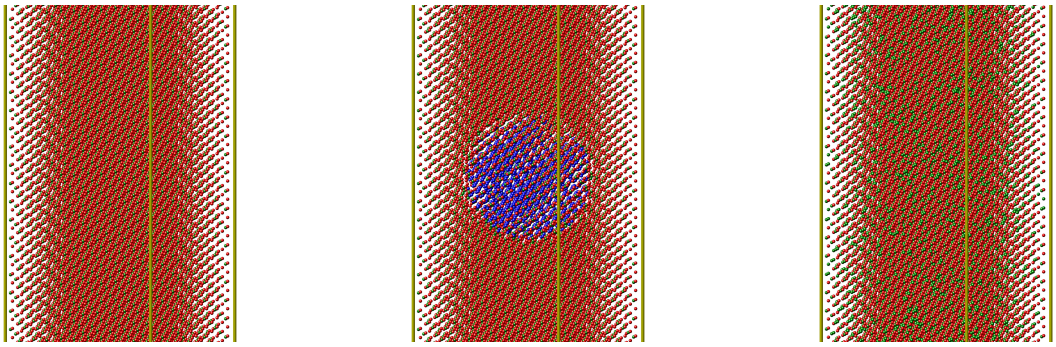

Fig. 5.4: Visual representation of the system of pure Mg_2Si (left), Mg_2Si with 8 Si NP (center), and Mg_2Si with substitutional Si atoms matching the stoichiometry of 8 Si NP system (right). The Mg atoms are colored red, the Si atoms green, and the Si atoms in the NP are colored blue. The yellow lines are the edges of the simulation box.

An extended modified embedded atom method (MEAM) potential developed by Zhang [23] was implemented in order to describe the interatomic potentials of Mg_2Si as well as

its changes in stoichiometry. Eqn. 5.8 [1] describes how this potential is implemented using LAMMPS.

$$E_{sys} = \sum_i \left\{ F_i(\bar{\rho}_i) + \frac{1}{2} \sum_{i \neq j} \phi_{ij}(r_{ij}) \right\} \tag{5.8}$$

where E_{sys} is the total energy of a system of atoms, F_i is the embedding energy as a function of $\bar{\rho}_i$, $\bar{\rho}_i$ is the atomic electron density, ϕ_{ij} is a pair potential interaction as a function of r_{ij}, i refers to the atom in question, j refers to the neighboring atoms of i, and r_{ij} is the distance between atoms i and j.

The extended MEAM potential contains files with information that represents the potentials of the many possible stoichiometries of Mg_2Si, and so different potential information was used for different stoichiometries. For the pure Mg_2Si case, the potential information specifically designated for that stoichiometry was used. In the case of the Mg_2Si with Si NPs, the same potential information used for pure Mg_2Si for the matrix material, as well as the potential information describing pure Si for the Si NPs, was applied. When matching the stoichiometry of the Si NP simulations with random substitutions of Mg atoms for Si atoms, the same potential information used for pure Mg_2Si was once again applied. This assignment of potentials was based on the assumption of little difference between these cases due to the theoretically even distribution of the Si atoms and the similar a/o Si value to pure Mg_2Si. This has been proved in part by the stability of the system despite the high T_{eq} (900 K) and greater a/o Si.

Each simulation was run for a total of 15 ns to ensure that the systems reached steady state. The 15 ns were divided so that most of the time was given to the constant heat flux application: NPT, NVT, and NVE each ran 0.6 ns, then the NVE continued while the constant heat flux was applied for another 2.0 ns, and the remaining 11.2 ns were used to record temperature gradients every 0.2 ps or 0.02 ps, while the NVE and constant heat flux continued to run. Each of the systems involving pure Mg_2Si, Mg_2Si with Si NPs, and Mg_2Si with substitutional Si atoms, were simulated at T_{eq} of 300, 600, and 900 K, and at an equilibration pressure of 0.0 bars. In almost all the Si NP and random Si substitutional

simulations, it was necessary to decrease the timestep size in order to maintain the stability of the system of atoms in the simulation box. The increase of the T_{eq}, a/o Si, and number of Si NPs in the systems all made it necessary to decrease the timestep size, which was done by a factor of 10.

The temperature values composing the temperature gradient were collected in the following way. The temperature values were averaged both temporally and spatially, being determined by a time increment to be averaged over as well as a 3-dimensional space to be averaged over. The 3- dimensional space, or chunk is determined by a length value, which is used to break up the Mg_2Si test section into rectangular prisms along the z-direction, with divisions being perpendicular to the z-direction every certain chunk size length value. Time increments values of 0.2 ps or 0.02 ps (for the simulations with the smaller timestep) were used in their respective simulations, while the chunk size value of 50 Å was used in all simulations. Using the aforementioned averaging process, the occurrence of steady state in these average temperature values was identified. The average temperature values were averaged over the time from the beginning of steady state until the end of the simulation. This process, which was repeated for each system, provided a temperature gradient for the entire Mg_2Si test section. Eqn. 5.7 was then used to calculate the λ_p of each system. This equation was used over 11 chunks to obtain a more accurate temperature gradient, and thus a more accurate value for λ_p.

CHAPTER 6

Results and Discussion

6.1 SWCNT

In order complete a basic verification of the validity of the interatomic potential, the 200 nm SWCNT system was simulated at T_{eq} of 300 K. This resulted in a λ_p of 2.457×10^4 $Wm^{-1}K^{-1}$, which when circle method for A, gives a value of 8.335×10^3 $Wm^{-1}K^{-1}$, falling within the range of the values reported in Table 1.2, and those reported by Lukes et al [11]. As no information in the table indicates the method of area calculation, this value may fall outside the range of most of the values. However, the perfect crystallinity of the system considerably enhances λ_p. From this point, this, and the other SWCNT systems were simulated at the aforementioned T_{eq} values.

The highest value of λ_p was 3.940×10^4 (A using circle method: 1.337×10^4) $Wm^{-1}K^{-1}$, and was found in the 200 nm SWCNT system at a T_{eq} of 50 K. The lowest value of λ_p was 933.2 (A using circle method : 316.7) $Wm^{-1}K^{-1}$, and was found in the 25 nm SWCNT system at a T_{eq} of 50 K. These values, and all others for the various T_{eq}, lengths, and diameters applied to the SWCNTs, are very high, which is characteristic of SWCNTs (see Table 1.2). These values may still seem high, but this may be attributed, at least in part, to the perfect crystallinity of the SWCNT systems simulated. More information on the results can be found in Figure 6.1 and Figure 6.2

The fact that the lowest value for λ_p comes from the shorts length SWCNT tested makes sense, as the longer wavelength phonons that tend to carry more heat are not allowed in such a short system [3]. However, this value would normally be expected to occur at the highest T_{eq} value used, not the lowest. This is typically an incorrect artifact of LAMMPS, as it assumes a classiscal Dulong and Petit model in which λ_p essentially goes to infinite $Wm^{-1}K^{-1}$ as T_{eq} goes to 0 K (assuming the length in the direction of the heat flux is long

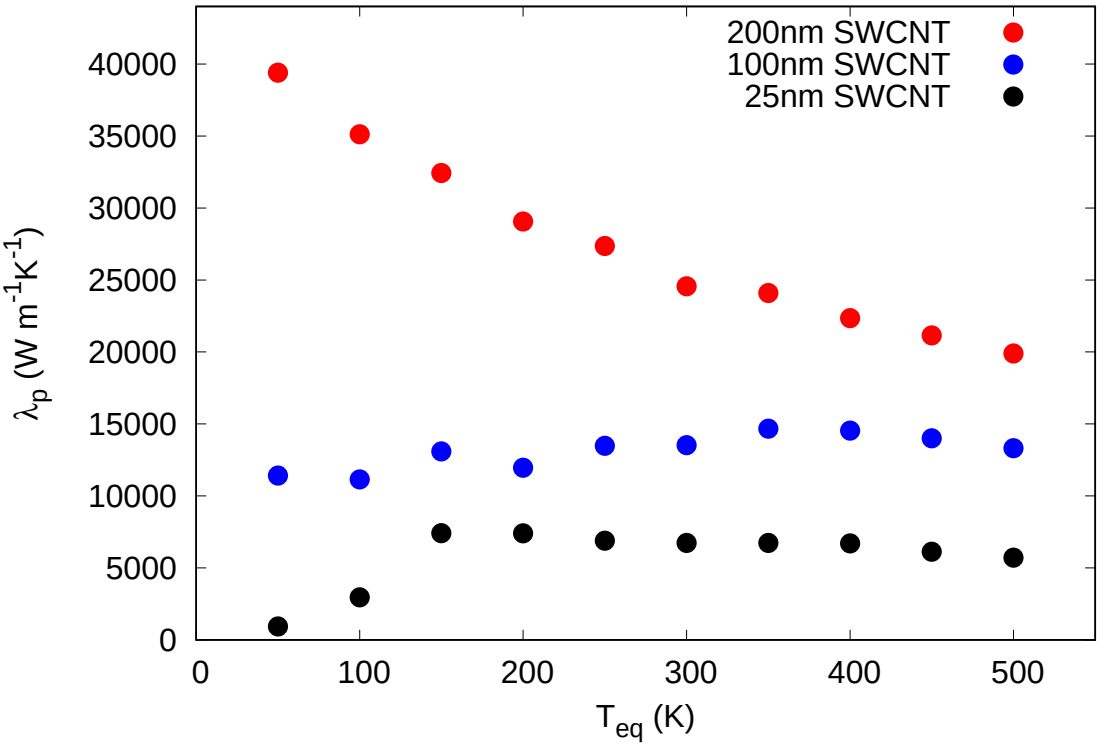

Fig. 6.1: λ_p vs. T_{eq} for SWCNT systems of lengths of 25, 100, and 200 nm.

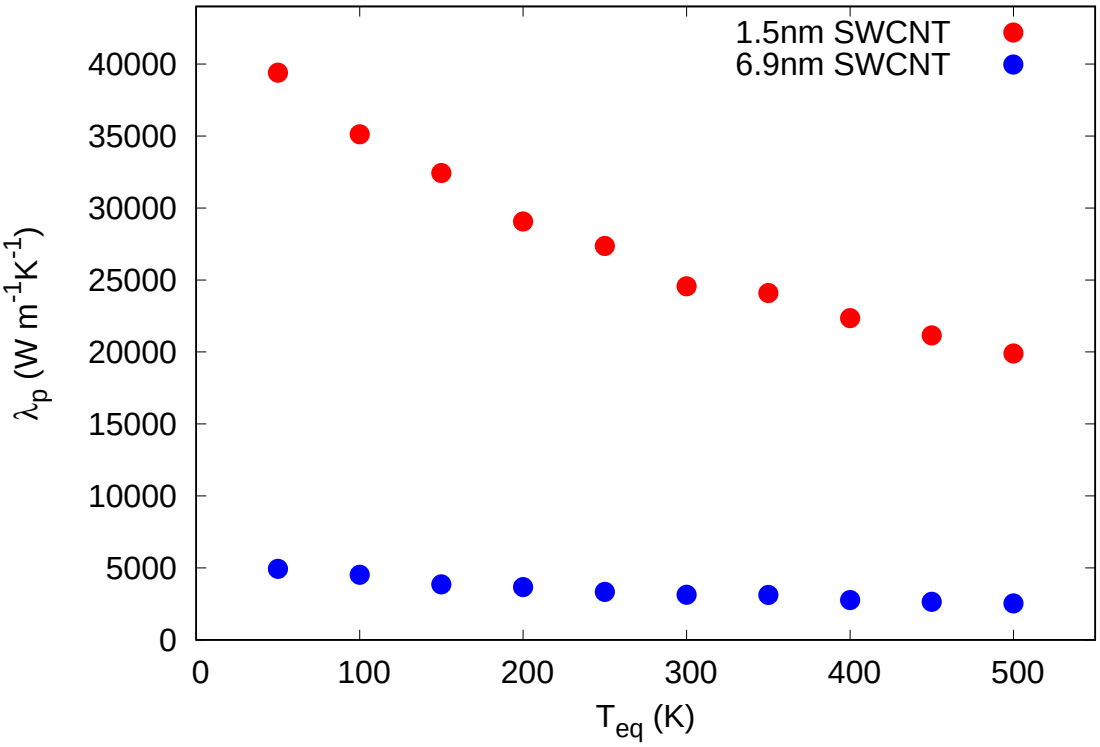

Fig. 6.2: λ_p vs. T_{eq} for SWCNT systems of diameters of 1.5 and 6.9 nm.

enough). From Figure 6.1 and Figure 6.2, it is easy to see that only the 200 nm SWCNT system seems to exhibit this behavior. Ironically, though the this is the only system whose λ_p behaves the way it should according to LAMMPS, this also means that this is the system with the least accurate results when compared with what would be expected for experimental results.

One possible explanation for the apparent deviation of λ_p to infinite $Wm^{-1}K^{-1}$ as T_{eq} goes to 0 K is that λ_p is not actually following that trend, but instead will peak and then decrease, approaching a value of 0 $Wm^{-1}K^{-1}$ as T_{eq} goes to 0 K, just as plots of λ_p vs T_{eq} for most materials do [34].

The mechanism that likely causes λ_p to decrease at T_{eq} increases is multi-phonon scattering. As T_{eq} increases, the phonon population increases, and so more scattering between phonons, or multi-phonon scattering, occurs, thus impeding λ_p. The mechanism that likely causes the decrease in λ_p as T_{eq} decreased, seen from Figure 6.1 only in the 25 and 100 nm SWCNT systems, is suppression of long-wavelength phonons due to the length of these systems in the direction of the applied heat flux.

Other general trends in Figure 6.1 and Figure 6.2 are that increase in SWCNT length leads to an increase in the value of λ_p, and that an increase in the diameter of SWCNTs leads to a decrease in λ_p values. These results regarding changes in length were generally expected.

Figure 6.3, adapted from Saito et al [35] shows the phonon dispersion and phonon density of states plots for SWCNT. The slopes of each of the lines in the phonon dispersion plot (left) can be taken as the propagating velocity, through the material, of the associated normal phonon mode.

It can be seen from this figure that there are many long-wavelength phonons with high velocities. These long-wavelength phonons can only exist where length of the SWCNT at least half their wavelength, and they tend to transfer heat much better due to their high propagating velocities, and their longer phonon lifetimes, or time that they exist before scattering. Therefore, as the length of the SWCNT system increased, more of these phonons

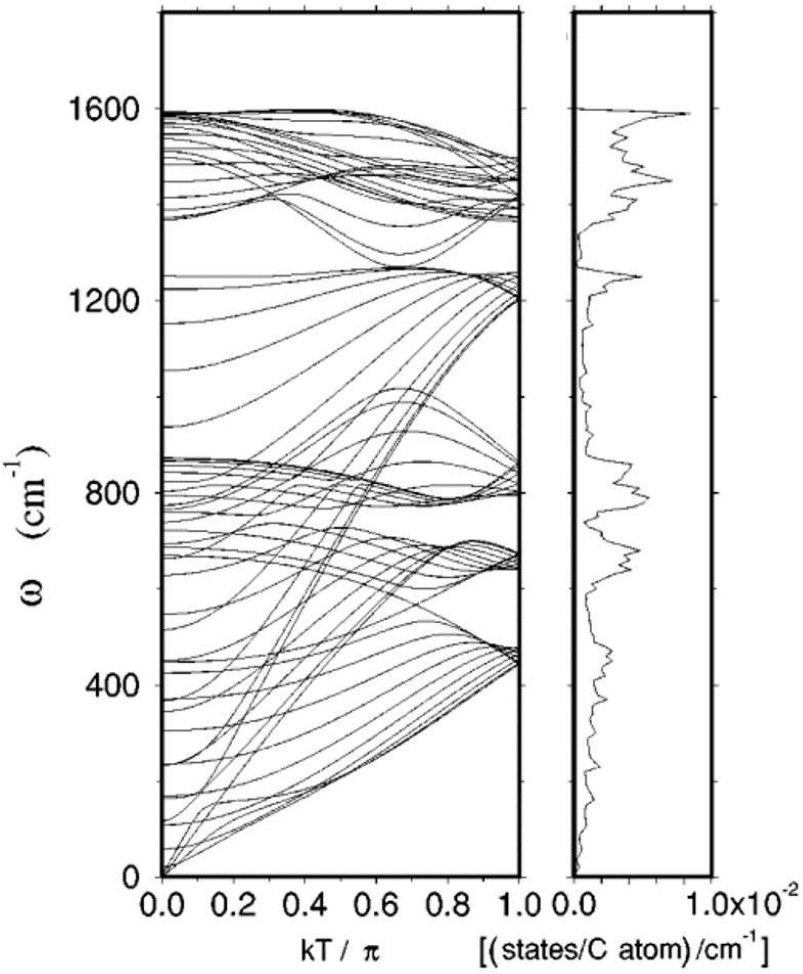

Fig. 6.3: Phonon dispersion and phonon density of states plots for SWCNT (adapted from [35]).

with longer lifetimes and higher velocities [3] populated the SWCNT. The higher population of these phonons, often known as acoustic phonons, led to higher values of λ_p.

Increases in diameter resulted in increases in A, however, this work was only considering A that included the physical material. This means that as A increases, so does volume of the material, thus decreasing dT per unit length. In view of Eqn. 5.7, the increase in A and decrease in dT should cancel any effects on the value of λ_p. Therefore the drop in λ_p seen in Figure 6.2 cannot be attributed to the SWCNTs changes in diameter and the resulting changes in A.

One explanation is given by Yue et al [25]. In their work, they found that the optical phonon population increased, specifically in the lower optical phonon frequencies, with increase in the diameter of the SWCNTs. This resulted in more optical-acoustic scattering processes, leading to decreasing λ_p values as SWCNT diameter increased. Their values for λ_p and diameters at which these values were calculated do not match those of this work, which can be attributed to differences in the interatomic potential used.

6.2 Mg_2Si

First, a value for λ_p of pure Mg_2Si at 300 K was calculated, which resulted in a λ_p of 8.454 $\pm$ 1.094 $Wm^{-1}K^{-1}$. Since this value is comparable to the experimental value of 7.8 $Wm^{-1}K^{-1}$ found by LaBotz, R [10], the aforementioned geometry and potential information was used to proceed. λ_p relating to changes the mean free path (Λ) can be calculated using Eqn. 6.1 [36]:

$$\lambda_p = \frac{1}{3}\Lambda C v \tag{6.1}$$

where C is the heat capacity and v is the average speed of phonons through a given material. This v was calculated using a linear approximation of the acoustic branches from the X point to the Γ point (see Figure 6.4, adapted from [37]), thus giving a higher-than-average group phonon velocity. This was not the average velocity of all of the phonons, as v should be, but was instead an estimation. The value for C was taken from [38] and converted

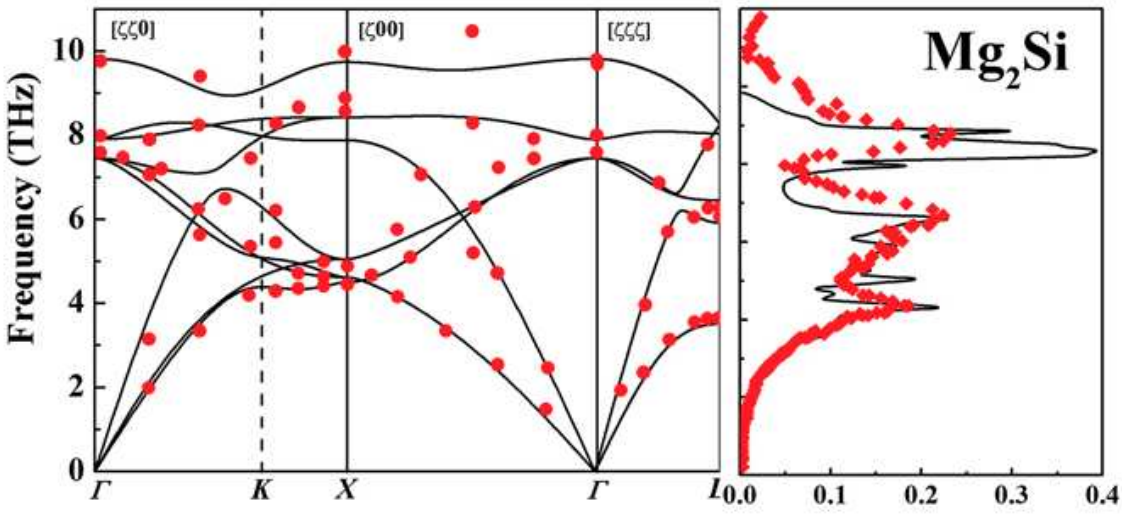

Fig. 6.4: Phonon dispersion and phonon density of states plots for Mg_2Si (adapted from [37]). Experimental points along the phonon dispersion plot are from [39] and [40], represented by solid red circles. Experimental points along the phonon density of states are from [41], represented by solid red diamonds.

using the density and molecular mass of Mg_2Si. The value for Λ was calculated using Eqn. 6.1, using the aforementioned values for v and C, and using λ_p from the simulation of pure Mg_2Si at T_{eq} of 300 K. The values for Λ were adjusted for taking into account the ratio of an Si NP's projection compared to that of the surrounding Mg_2Si, the number of Si NPs, and their associated spacing. With this, the 16 Si NP Mg_2Si system still needed to be adjusted. The finished product of these efforts can be seen in Figure 6.5. All of this was done, including the many estimations and adjustments, so that the trend could be seen on the graph, and so that it could give realistic results. Though many estimations had been done, the general trend of the theoretical and computational plots of λ_p in Figure 6.5 appear to agree.

The lowest λ_p for the Mg_2Si systems with Si NPs at T_{eq} of 300 K was 1.791 $\pm$ 0.124 $Wm^{-1}K^{-1}$, resulting from the system with 16 Si NPs (an equivalent stoichiometry of 49.55 a/o Si). This same nanostructure also resulted in the lowest λ_p for the Mg_2Si systems with Si NPs at T_{eq} of 600 and 900 K, with values of 1.649 $\pm$ 0.157 and 1.280 $\pm$ 0.214 $Wm^{-1}K^{-1}$. For further information on the λ_p of Mg_2Si systems with Si NPs, see Figure 6.5

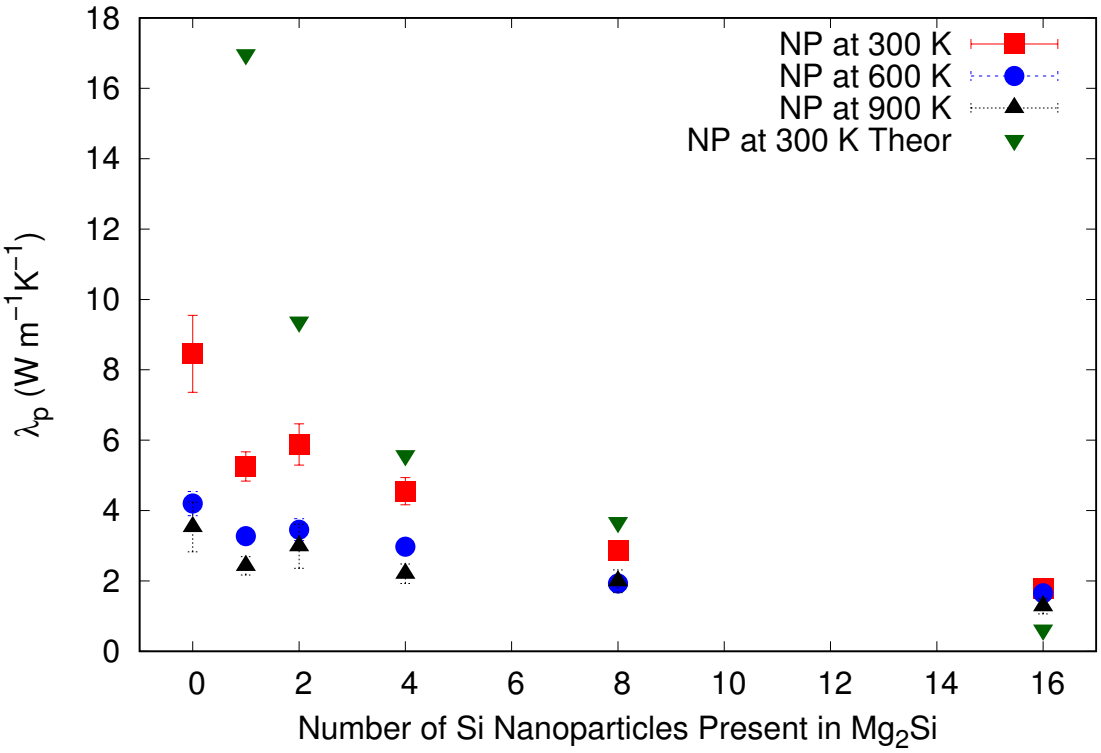

Fig. 6.5: λ_p vs. number of Si NPs present in Mg_2Si systems at T_{eq} values of 300, 600, and 900 K, representing Mg_2Si systems with 0, 1, 2, 4, 8, and 16 Si NPs, respectively. Included is an estimation of λ_p for the T_{eq} of 300 K case, using Eqn. 6.1 [36], denoted by Si NP at 300 K Theor.

and Figure 6.6.

The lowest λ_p for the Mg_2Si systems with dispersed Si atoms at T_{eq} of 300 K was 1.300 $\pm$ 0.053 $Wm^{-1}K^{-1}$, resulting from the 49.55 a/o Si system. This same nanostructure also resulted in the lowest λ_p for the Mg_2Si systems with dispersed Si atoms at T_{eq} of 600 and 900 K, with values of 1.064 $\pm$ 0.117 and 0.9347 $\pm$ 0.292 $Wm^{-1}K^{-1}$. This last value was the lowest overall. For more information on the λ_p of Mg_2Si systems with dispersed Si atoms, see Figure 6.7 and Figure 6.8.

From Figure 6.5 and Figure 6.7, it is easy to see that, as predicted, λ_p decreased as a/o Si and the number of Si NPs in Mg_2Si increased. It is interesting to note that λ_p decreased with diminishing returns, roughly following an asymptotic decay, as both the number of Si NPs and the a/o Si in Mg_2Si increased. However, the data from the dispersed Si atom

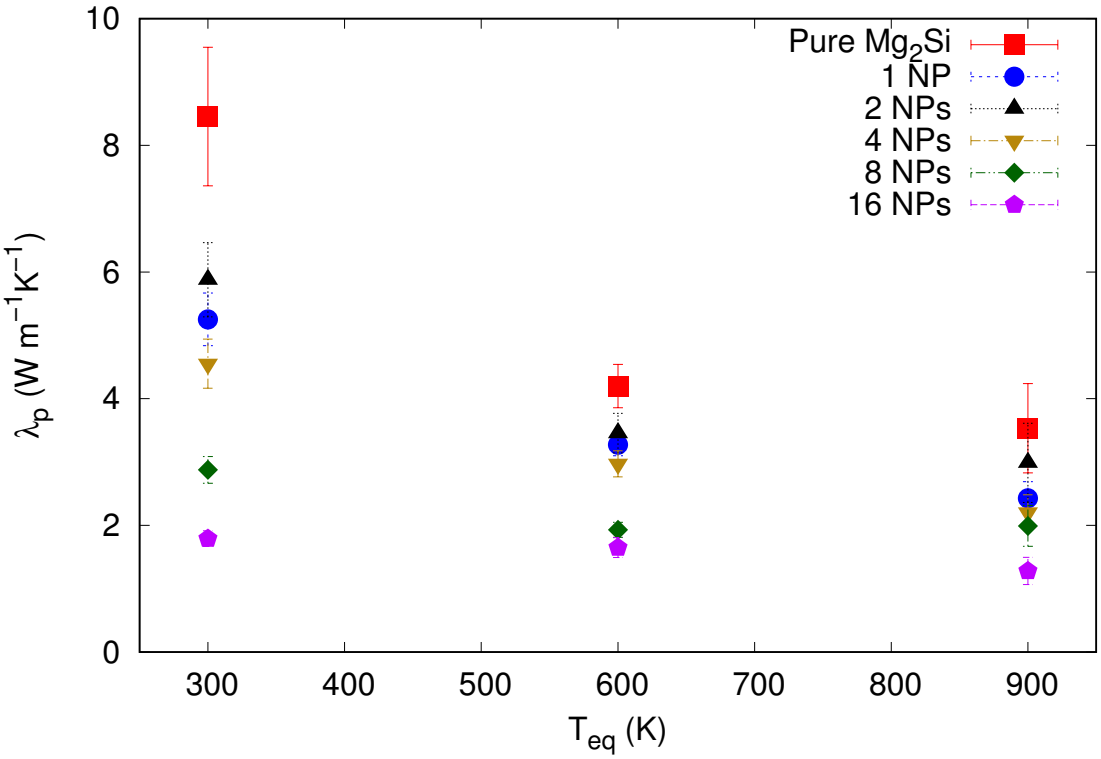

Fig. 6.6: λ_p vs. T_{eq} for pure Mg_2Si (0 Si NPs) and Mg_2Si systems with 1, 2, 4, 8, and 16 Si NPs

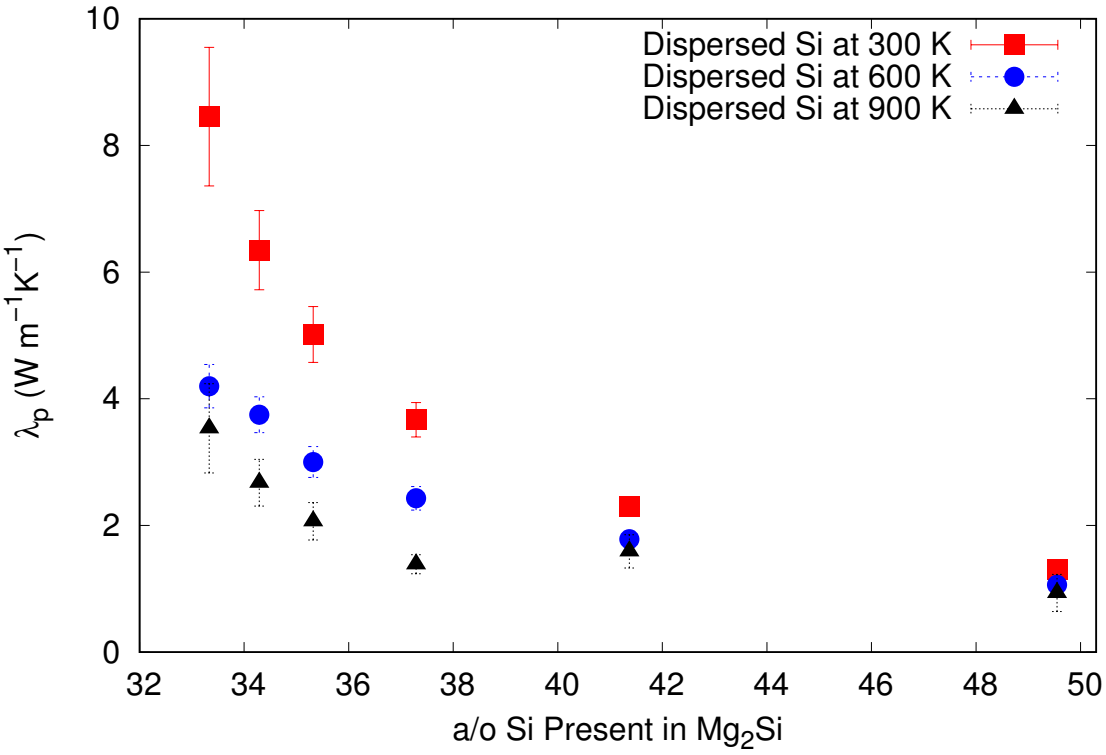

Fig. 6.7: λ_p vs. a/o Si present in Mg_2Si systems at T_{eq} values of 300, 600, and 900 K. The a/o Si values correspond to the stoichiometry of the system of pure Mg_2Si (33.33 a/o Si), and respective systems of Mg_2Si having 1, 2, 4, 8, and 16 Si NPs.

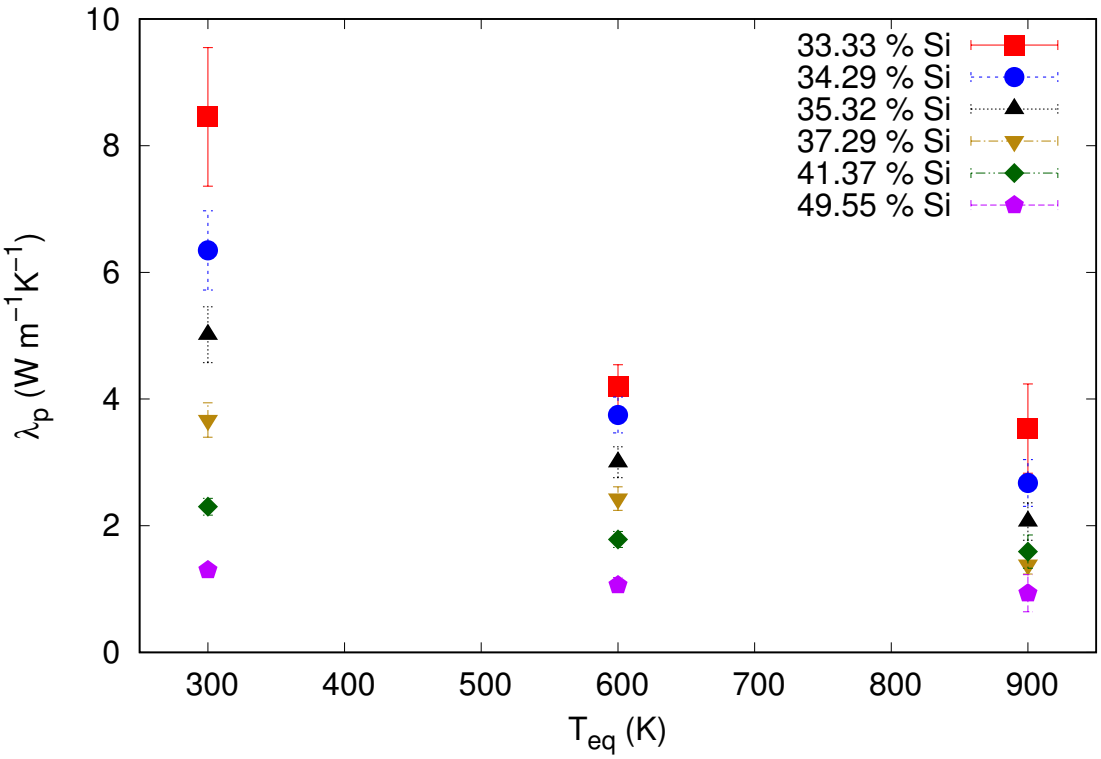

Fig. 6.8: λ_p vs. T_{eq} for Mg_2Si systems with substitutional Si atoms, respectively matching the stoichiometry of the Mg_2Si systems with 0 (pure Mg_2Si), 1, 2, 4, 8, and 16 Si NPs.

method seemed to more closely resemble an asymptotic decay when compared to the data of the Si NP method. In Figure 6.6 and Figure 6.8, the effect of T_{eq} on λ_p declines as NP count increases because the phonons whose propagation the higher T_{eq} would normally hinder have, as the NP concentration increases, already been hindered due to boundary resistance.

6.2.1 Reduction in λ_p in 1 Si NP Case

As can be seen in From Figure 6.5, the λ_p of the 1 Si NP cases for each T_{eq} are consistently lower than that of their 2 Si NP counterparts, a clear break from the trend of the rest of the data. The 1 Si NP case had its sole Si NP in the center of the simulation box, directly half way between the hot and cold sections. Because of this, it was thought bringing the 2 Si NPs in the 2 Si NP at 300 K T_{eq} case closer to the center of the simulation box could provide a better approximation of the 1 Si NP at 300 K T_{eq} case whose Si NP was at the center of its simulation box. Then the λ_p of this new simulation set up could be compared with the λ_p of the original set up for the 2 Si NP case, and it would be clear to see whether the concentration of the Si NPs at the center of the simulation box effected λ_p. The new system of 2 Si NPs had the spacing between them decreased from 405.6 to 215.5 Å. This new system was run, resulting in a λ_p of 4.403 $Wm^{-1}K^{-1}$, as opposed to that of the original, 5.877 $Wm^{-1}K^{-1}$. This seems to imply that as Si NPs are more concentrated at the halfway point between heat sink and heat source, the λ_p values decrease, despite no change in stoichiometry. Since the 1 Si NP case has the Si NP placed directly at the center of the simulation, it seems to make sense that this specific set of 1 Si NP simulations with the NP at the center of the simulation box result in lower than expected values for λ_p.

CHAPTER 7

Conclusion

7.1 SWCNT

The major results from the work with SWCNTs are that increases in length and decreases in diameter increase resulting values of SWCNT λ_p. Another interesting result is that as SWCNT length increases, the peak λ_p value occurs at a lower and lower T_{eq}. All of these results, especially the latter, need more simulations to obtain more concrete conclusions. More systems of SWCNT should be simulated between lengths of 0 and 200 nm, between diameters of 0 and 6.9 nm, and between T_{eq} of 0 and 50 K. These simulations should give enough information to better conclude whether the results are an artifact of the interatomic potential, LAMMPS, or perhaps worth experimental verification.

7.2 Mg_2Si

The first major result from this work is that increasing the a/o Si in a Mg2Si system, whether through addition of Si NPs or dispersed Si atoms, decreases λ_p. This is of course only true to a certain a/o of Si in Mg_2Si, as diminishing reductions in λ_p occur as a/o Si in Mg_2Si increases.

Comparing the two methods of a/o Si addition, the systems of Mg_2Si with atomically dispersed Si tend to have the lower values λ_p. This may have to do with the mass difference between Si and Mg, or the fact that the Si substitutionals are spaced such that they decrease the Λ of Mg_2Si. In the Si NP method, boundary resistance seems to have a greater effect on λ_p reduction when Si NP concentrations are smaller, such as the 1 and 2 NP cases, than the decrease in Λ does on λ_p reduction.

As mentioned previously, experimental work will be necessary as a later step to verify that the ZT increases in systems arranged according to this work significantly enough for

application.

7.3 Summary Conclusion

SWCNT and Mg_2Si are very different for many reasons. Besides the one being a NP, and the other a material in the original sense of the word, the first is generally valued due to its high λ_p, while the value of Mg_2Si increases as methods to decrease its λ_p are discovered. For both materials, information was recovered that was generally expected, and that generally agrees with experimental results. For example increasing the length of SWCNT system increases the resulting λ_p. Also, increasing the a/o Si in Mg_2Si systems decreases the resulting λ_p. For both systems, it was expected that λ_p would decrease as T_{eq} increased, which was also generally true. Both material systems also had interesting unexpected results, such as the shift in the peak of values for λ_p of the 200 nm length SWCNT, or the case of the lower than expected λ_p value for the Mg_2Si with one Si NP.

These results, when compared to their respective experimental results, seem to imply at least two things. First, that MD simulations struggle with accuracy of individual values and therefore are prone to produce artifacts in the results. Second, and somewhat in contrast, that MD simulations can produce results close to experimental results, in some cases, and often agree with trends found experimentally. Combining these two points, MD simulations are used most effectively in finding trends in data, maybe even showing promising areas of experimental research, as long as their limitations and potential for unrealistic results are understood.

For this specific work, and as mentioned in part before, further work could be done on SWCNTs with T_{eq} values closer to 0 K, a greater number of different diameters and lengths, and even different potential functions. Mg_2Si, however, may be a candidate for a few experimental measurements of the λ_p, as well as σ, of the stoichiometries that seem to lower λ_p the most. Some MD simulations could be run as well regarding the reduction in λ_p in 1 Si NP to discover the potential artifact in either the LAMMPS code, the extended MEAM potential used, or the reality of human error that caused this result.

REFERENCES

[1] S. Plimpton, "Fast parallel algorithms for short-range molecular dynamics," *Journal of Computational Physics*, vol. 117, pp. 1–19, 1995.

[2] X. Wang, H. Lee, Y. Lan, G. Zhu, G. Joshi, D. Wang, J. Yang, A. Muto, M. Tang, J. Klatsky, S. Song, M. Dresselhaus, G. Chen, and Z. Ren, "Enhanced thermoelectric figure of merit in nanostructured n-type silicon germanium bulk alloy," *Applied Physics Letters*, vol. 93, no. 193121, 2008.

[3] P. K. Schelling, S. R. Phillpot, and P. Keblinski, "Comparison of atomic-level simulation methods for computing thermal conductivity," *Physical Review B*, vol. 65, p. 144306, April 2002.

[4] A. J. H. McGaughey and M. Kaviany, "Thermal conductivity decomposition and analysis using molecular dynamics simulations: Part ii. complex silica structures," *International Journal of Heat and Mass Transfer*, vol. 47, pp. 1799–1816, April 2004.

[5] J. M. Larkin and A. J. H. McGaughey, "Thermal conductivity accumulation in amorphous silica and amorphous silicon," *Physical Review B*, vol. 89, p. 144303, April 2014.

[6] C. Choi, W. T. Yorgason, and N. Roberts, "Prediction of thermal boundary conductance at the interface with phonon wave-packet simulations: The roles of vibrational spectra differences, interface bond strength, and inelastic scattering," *ASME, Heat Transfer Summer Conference*, vol. 1, no. 1, pp. V001T02A003–V001T02A003, July 2016.

[7] X. Gu and R. Yang, "Phonon transport and thermal conductivity in two-dimensional materials," *Annual Review of Heat Transfer*, vol. 19, pp. 1–65, 2016.

[8] A. J. H. McGaughey and J. M. Larkin, "Predicting phonon properties from equilibrium molecular dynamics simulations," *Annual Review of Heat Transfer*, vol. 17, pp. 49–87, 2014.

[9] A. McGaughey and M. Kaviany, "Thermal conductivity decomposition and analysis using molecular dynamics simulations. part I. lennard jones argon," *International Journal of Heat and Mass Transfer*, vol. 47, 2004.

[10] R. J. LaBotz and D. R. Mason, "The thermal conductivities of mg2si and mg2ge," *Journal of The Electrochemical Society*, vol. 110.2, pp. 121–126, 1963.

[11] J. R. Lukes and H. Zhong, "Thermal conductivity of individual single-wall carbon nanotubes," *Journal of Heat Transfer*, vol. 129, no. 6, pp. 705–716, June 2007.

[12] M. A. Osman and D. Srivastava, "Temperature dependence of the thermal conductivity of single-wall carbon nanotubes," *Nanotechnology*, vol. 12, pp. 21–24, 2001.

[13] J. Che, T. agin, and I. Goddard, W. A., "Thermal conductivity of carbon nanotubes," *Nanotechnology*, vol. 11, pp. 65–69, 2000.

[14] Z. Yao, J. Wang, B. Li, and G. Liu, "Thermal conductivity of carbon nanotubes using molecular dynamics," *Phys. Rev. B*, vol. 71, p. 085417, Feb 2005.

[15] C. W. Padgett and D. W. Brenner, "Influence of chemisorption on the thermal conductivity of single-wall carbon nanotubes," *Nano Lett.*, vol. 4, pp. 1051–1053, May 2004.

[16] J. F. Moreland, J. B. Freund, and G. Chen, "The disparate thermal conductivity of carbon nanotubes and diamond nanowires studied by atomistic simulation," *Microscale Thermophys. Eng.*, vol. 8, pp. 61–69, 2004.

[17] S. Maruyama, "A molecular dynamics simulation of heat conduction of a finite length single-walled carbon nanotube," *Microscale Thermophys. Eng.*, vol. 7, pp. 41–50, 2003.

[18] N. Mingo and D. A. Broido, "Length dependence of carbon nanotube thermal conductivity and the "problem of long waves"," *Nano Letters*, vol. 5, no. 7, pp. 1221–1225, June 2005.

[19] C. H. Yu, L. Shi, Z. Yao, D. Y. Li, and A. Majumdar, "Thermal conductance and thermopower of an individual single-wall carbon nanotube," *Nano Lett.*, vol. 5, pp. 1842–1846, Jul 2005.

[20] E. Pop, D. Mann, Q. Wang, K. Goodson, and H. Dai, "Influence of chemisorption on the thermal conductivity of single-wall carbon nanotubes," *Nano Lett.*, vol. 6, pp. 96–100, Dec 2006.

[21] J.-L. Zang, Q. Yuan, F.-C. Wang, and Y.-P. Zhao, "A comparative study of youngs modulus of single-walled carbon nanotube by cpmd, md and first principle simulations," *Computational Materials Science*, vol. 43, pp. 621–625, September 2009.

[22] W. Humphrey, A. Dalke, and K. Schulten, "VMD – Visual Molecular Dynamics," *Journal of Molecular Graphics*, vol. 14, pp. 33–38, 1996.

[23] H. Zhang, T. Zheng, B. Gnade, and K. Cho, "The effect of point defects and nanoparticles on thermal conductivity of magnesium silicide," *Computational Materials Science*, vol. 104, pp. 172–176, June 2015.

[24] Z. Han and A. Fina, "Thermal conductivity of carbon nanotubes and their polymer nanocomposites: A review," *Progress in Polymer Science*, vol. 36, pp. 914–944, 2011.

[25] S.-Y. Yue, T. Ouyang, and M. Hu, "Diameter dependence of lattice thermal conductivity of single-walled carbon nanotubes: Study from ab initio," *Scientific Reports*, vol. 5, p. 15440, October 2015.

[26] S. S. Lee, C. Zhang, Z. A. Lewicka, M. Cho, J. T. Mayo, W. W. Yu, R. H. Hauge, and V. L. Colvin, "Control over the diameter, length, and structure of carbon nanotube carpets using aluminum ferrite and iron oxide nanocrystals as catalyst precursors," *Journal of Physical Chemistry C*, vol. 116, p. 1028710295, March 2012.

[27] W. T. Yorgason, A. N. Barnes, and N. Roberts, "Improvement of thermoelectric properties through reduction of thermal conductivity by nanoparticle addition and stoichiometric change to mg2si," *MRS Advances*, vol. 2, pp. 3637–3643, August 2016.

[28] W. Kim, J. Zide, A. Gossard, D. Klenov, S. Stemmer, A. Shakouri, and A. Majumdar, "Thermal conductivity reduction and thermoelectric figure of merit increase by embedding nanoparticles in crystalline semiconductors," *Physical Review Letters*, vol. 96, p. 045901, February 2006.

[29] P. Boulet, M. J. Verstraete, J.-P. Crocombette, M. Briki, and M.-C. Record, "Electronic properties of the mg2si thermoelectric material investigated by linear-response density-functional theory," *Computational Materials Science*, vol. 50.3, pp. 847–851, 2011.

[30] Z.-G. Chen, G. Han, L. Yang, L. Cheng, and J. Zou, "Nanostructured thermoelectric materials: Current research and future challenge," *Progress in Natural Science: Materials International*, vol. 22, no. 6, pp. 535–549, December 2012.

[31] A. Azaddin, R. Ayub, A. Azman, M. M. Arshad, M. Fathil, U. Hashim, A. Ruslinda, S. C. Gopinath, C. Voon, and K. Foo, "The effect of aluminum nanoparticle on the seebeck coefficient of biomedical thermoelectric devices," in *Micro and Nanoelectronics (RSM), 2015 IEEE Regional Symposium on*. IEEE, 2015, pp. 1–4.

[32] C. Kim, S. Kim, Y.-K. Hong, M.-W. Oh, and M.-H. Jung, "Correlation between the magnetic and thermoelectric properties in mg2-xmnxsi," *Journal of Alloys and Compounds*, vol. 690, pp. 51–56, January 2017.

[33] N. A. Roberts, D. G. Walker, and D. Y. Li, "Molecular dynamics simulation of thermal conductivity of nanocrystalline composite films," *International Journal of Heat and Mass Transfer*, vol. 52, March 2009.

[34] P. Debye, "Zur theorie der spezifischen wärmen," *Annalen der Physik*, vol. 344, pp. 789–839, 1912.

[35] R. Saito, T. Takeya, T. Kimura, G. Dresselhaus, and M. S. Dresselhaus, "Raman intensity of single-wall carbon nanotubes," *Physical Review B*, vol. 57, no. 7, pp. 4145–4153, Feb. 1998.

[36] G. Chen, "Thermal conductivity and ballistic-phonon transport in the cross-plane direction of superlattices," *Phys. Rev. B*, vol. 57, pp. 14 958–14 973, Jun 1998.

[37] X. Liu, Y. Wang, J. O. Sofo, T. Zhu, L.-Q. Chen, and X. Zhao, "First-principles studies of lattice dynamics and thermal properties of mg2si1xsnx," *Journal of Materials Research*, vol. 30, pp. 2578–2584, September 2015.

[38] O. Madelung, U. Rssler, and M. Schulz, "Magnesium silicide (mg2si) debye temperature, heat capacity, density, melting point," in *Non-Tetrahedrally Bonded Elements and Binary Compounds I*. Springer, 1998, pp. 1–4.

[39] M. T. Hutchings, T. W. D. Farley, M. A. Hackett, W. Hayes, S. Hull, and U. Steigenberger, "Neutron scattering investigation of lattice dynamics and thermally induced

disorder in the antifluorite mg2si," *Solid State Ionics*, vol. 28, pp. 1208–1212, September 1988.

[40] R. J. Kearney, T. G. Worlton, and R. E. Schmunk, "Lattice dynamics of magnesium stannide at room temperature," *Journal of Physics and Chemistry of Solids*, vol. 31, pp. 1085–1097, May 1970.

[41] D. Bessas, R. E. Simon, K. Friese, M. Koza, and R. P. Hermann, "Lattice dynamics in intermetallic mg2ge and mg2si," *Journal of Physics: Condensed Matter*, vol. 26, p. 485401, November 2014.

APPENDICES

APPENDIX A

Sample LAMMPS MD Scripts

A.1 Sample LAMMPS MD Script for λ_p of SWCNT Systems

```
##–SIMULATION OF λ_p OF A SWCNT–##

##–SYSTEM INTIALIZATION–##

clear
echo both

units metal
dimension 3
atom_style molecular
boundary p p p
processors 1 1 1

##–DATA FILE INPUT–##

#read_data data4Mol_200nm.txt
#read_data Mol_data4_100nm.txt
read_data Mol_data4_25nm.txt

##–REGION SETUP–##

region wall1 block -50 50 -50 50 -1 20 units box
region cold block -50 50 -50 50 20 41 units box
region tube block -50 50 -50 50 41 208 units box
region hot block -50 50 -50 50 208 229 units box
region wall2 block -50 50 -50 50 229 251 units box

##–INTERATOMIC POTENTIAL INFORMATION–##

bond_style harmonic
bond_coeff 1 20.81443 1.340
angle_style harmonic
angle_coeff 1 3.902706 119.9773623
dihedral_style harmonic
```

```
dihedral_coeff 1 0.13009 -1 2
improper_style cvff improper_coeff 1 0.016044458 -1 2

pair_style lj/cut 1
pair_coeff * * 1 1

mass * 12

##–GROUPING REGIONS–##

group wall1 region wall1
group wall2 region wall2
group cold region cold
group hot region hot
group tube region tube
group nowalls union cold tube hot

##–T_eq SET AND INITIALIZATION–##

variable t equal 50.0
timestep 0.001
thermo 200
neighbor 2.0 bin
neigh_modify every 3 delay 3
velocity nowalls create $t 49284121
thermo 200

##–NEMD EQUILIBRATION–##

fix 7 nowalls npt temp $t $t 10 iso 0.0 0.0 10
run 300000
unfix 7

fix 8 nowalls nvt temp $t $t 1
run 300000
unfix 8

fix 1 nowalls nve
variable g_ke equal ke(tube)
variable g_temp equal v_g_ke/1.5/8.617343e-5/19540
thermo 200
thermo_style custom step temp ke etotal v_g_temp
run 400000

##–CONSTANT HEAT FLUX APPLICATION–##
```

```
fix 3 cold heat 1 -0.625
fix 4 hot heat 1 0.625
compute coldBath cold temp
compute hotBath hot temp
thermo 200
thermo_style custom step temp ke etotal v_g_temp c_coldBath c_hotBath
run 100000

##–TEMPERATURE GRADIENT DATA COLLECTION–##


compute KE tube ke/atom

variable temp atom c_KE/1.5/8.617343e-5

compute 2 tube chunk/atom bin/1d z lower 25 units box

fix 5 tube ave/chunk 200 1 200 2 v_temp file tanner_imp_di_pair_style_lj_cut_10_pair_coeff_*_*_1_1_temp50_HF

run 900000
```

A.2 Sample LAMMPS MD Script for λ_p of Mg_xSi_x Systems

```
###SIMULATION OF λ_p OF Mg2Si WITH 2 Si NPs ###

##–SYSTEM INTIALIZATION–##

#clear
#echo both
units metal
dimension 3
atom_style atomic
boundary p p p

##–LATTICE INFORMATION AND REGION SETUP–##

lattice fcc 6.338

region box block 0 8 0 8 0 128 units lattice

variable h equal 2
variable s equal (64-($h/2))
variable e equal (64+($h/2))
variable g equal .25
```

```
variable a equal ($s-$g)
variable b equal ($e+$g)
variable r equal 3
variable R equal ($r+$g)

region wall1 block 0 8 0 8 0 7 units lattice
region cold block 0 8 0 8 7 14.5 units lattice
region uppertube block 0 8 0 8 14.5 64 units lattice
#region shield block 0 8 0 8 $a $b units lattice
#region nanoparticle block 0 8 0 8 $s $e units lattice
#region nanoparticle1 sphere 4 4 3.25 $r units lattice
#region shield1 sphere 4 4 3.25 $R units lattice
#region nanoparticle2 sphere 4 4 11.25 $r units lattice
#region shield2 sphere 4 4 11.25 $R units lattice
#region nanoparticle3 sphere 4 4 19.25 $r units lattice
#region shield3 sphere 4 4 19.25 $R units lattice
#region nanoparticle4 sphere 4 4 27.25 $r units lattice
#region shield4 sphere 4 4 27.25 $R units lattice
region nanoparticle5 sphere 4 4 35.25 $r units lattice
region shield5 sphere 4 4 35.25 $R units lattice
#region nanoparticle6 sphere 4 4 43.25 $r units lattice
#region shield6 sphere 4 4 43.25 $R units lattice
#region nanoparticle7 sphere 4 4 51.25 $r units lattice
#region shield7 sphere 4 4 51.25 $R units lattice
#region nanoparticle8 sphere 4 4 59.25 $r units lattice
#region shield8 sphere 4 4 59.25 $R units lattice
#region nanoparticle9 sphere 4 4 67.25 $r units lattice
#region shield9 sphere 4 4 67.25 $R units lattice
#region nanoparticle10 sphere 4 4 75.25 $r units lattice
#region shield10 sphere 4 4 75.25 $R units lattice
#region nanoparticle11 sphere 4 4 83.25 $r units lattice
#region shield11 sphere 4 4 83.25 $R units lattice
#region nanoparticle12 sphere 4 4 91.25 $r units lattice
#region shield12 sphere 4 4 91.25 $R units lattice
region nanoparticle13 sphere 4 4 99.25 $r units lattice
region shield13 sphere 4 4 99.25 $R units lattice
#region nanoparticle14 sphere 4 4 107.25 $r units lattice
#region shield14 sphere 4 4 107.25 $R units lattice
#region nanoparticle15 sphere 4 4 115.25 $r units lattice
#region shield15 sphere 4 4 115.25 $R units lattice
#region nanoparticle16 sphere 4 4 123.25 $r units lattice
#region shield16 sphere 4 4 123.25 $R units lattice
region lowertube block 0 8 0 8 64 113 units lattice
region hot block 0 8 0 8 113 120.5 units lattice
region wall2 block 0 8 0 8 120.5 128 units lattice
```

```
create_box 3 box
create_atoms 2 box

##–SI NP LATTICE INFORMATION AND CREATION–##

lattice sc 3.169 origin .5 .5 .5
create_atoms 1 box

#delete_atoms region shield1
#delete_atoms region shield2
#delete_atoms region shield3
#delete_atoms region shield4
delete_atoms region shield5
#delete_atoms region shield6
#delete_atoms region shield7
#delete_atoms region shield8
#delete_atoms region shield9
#delete_atoms region shield10
#delete_atoms region shield11
#delete_atoms region shield12
delete_atoms region shield13
#delete_atoms region shield14
#delete_atoms region shield15
#delete_atoms region shield16

lattice diamond 5.427
#create_atoms 3 region nanoparticle1
#create_atoms 3 region nanoparticle2
#create_atoms 3 region nanoparticle3
#create_atoms 3 region nanoparticle4
create_atoms 3 region nanoparticle5
#create_atoms 3 region nanoparticle6
#create_atoms 3 region nanoparticle7
#create_atoms 3 region nanoparticle8
#create_atoms 3 region nanoparticle9
#create_atoms 3 region nanoparticle10
#create_atoms 3 region nanoparticle11
#create_atoms 3 region nanoparticle12
create_atoms 3 region nanoparticle13
#create_atoms 3 region nanoparticle14
#create_atoms 3 region nanoparticle15
#create_atoms 3 region nanoparticle16

##–INTERATOMIC POTENTIAL INFORMATION–##
```

```
pair_style meam
pair_coeff * * newpotential.txt Mg Si Si6 mgsi.meam Mg Si Si6

##–GROUPING REGIONS–##

group wall1 region wall1
group wall2 region wall2
group cold region cold
group hot region hot
group uppertube region uppertube
group lowertube region lowertube
group nowalls union cold uppertube lowertube hot
group tube union uppertube lowertube

##–T_eq SET AND INITIALIZATION–##

timestep .001
restart 1000000 Restart_2multi_300K.*
dump 6 all xyz 10000000 xyzcoord_2multi_300K*.txt
variable t equal 300
thermo 200
neighbor 2.0 bin
neigh_modify every 3 delay 3
velocity nowalls create $t 49284121

##–NEMD EQUILIBRATION–##

fix 10 nowalls npt temp $t $t 10 iso 0.0 0.0 10
run 600000
unfix 10

fix 8 nowalls nvt temp $t $t 1
run 600000
unfix 8

timestep 0.0001
fix 1 nowalls nve
variable g_ke equal ke(tube)
variable g_temp equal v_g_ke/1.5/8.617343e-5/98305
thermo 200
thermo_style custom step temp ke etotal v_g_temp
run 6000000

##–CONSTANT HEAT FLUX APPLICATION–##
```

```
fix 3 cold heat 1 -0.19
fix 4 hot heat 1 0.19
compute coldBath cold temp
compute hotBath hot temp
thermo_style custom step temp ke etotal v_g_temp c_coldBath c_hotBath
run 20000000

##–TEMPERATURE GRADIENT DATA COLLECTION–##


compute KE tube ke/atom

variable temp atom c_KE/1.5/8.617343e-5

compute 2 tube chunk/atom bin/1d z lower 50 units box

fix 5 tube ave/chunk 200 1 200 2 v_temp file Mg2Si1_2multi_nanopart_300K_HG_2ns_HF0.19_Chsz50.txt

run 112000000
```

CURRICULUM VITAE

W. Tanner Yorgason

Published Journal Articles

- Improvement of Thermoelectric Properties through Reduction of Thermal Conductivity by Nanoparticle Addition and Stoichiometric Change to Mg_2Si, W. Tanner Yorgason, Arden N. Barnes, and Nicholas A. Roberts, *MRS Advances*, vol. 2, no. 58-59, pp. 3637-3643, 2017.

Published Conference Papers

- Prediction of Thermal Boundary Conductance at the Interface with Phonon Wave-Packet Simulations: The Roles of Vibrational Spectra Dierences, Interface Bond Strength, and Inelastic Scattering, ChangJin Choi, W. Tanner Yorgason, and Nicholas A. Roberts, *ASME Summer Heat Transfer Conference*, vol. 1, 2016.

Conference Presentations

- W. Tanner Yorgason and Nicholas A. Roberts, Size Dependent Thermal Conductivity of Single-Wall Carbon Nanotubes from Molecular Dynamics Simulations, *Materials Research Society Conference*, April 17-21 2017, Phoenix, AZ, USA. *(poster)*

- W. Tanner Yorgason, Arden Barnes, and Nicholas A. Roberts, Improvement of Thermoelectric Properties through Reduction of Thermal Conductivity by Nanoparticle Addition and Stoichiometric Change to Mg_2Si, *Materials Research Society Conference*, April 17-21 2017, Phoenix, AZ, USA. *(poster)*

- W. Tanner Yorgason, Arden Barnes, and Nicholas A. Roberts, Improvement of Thermoelectric Properties through Reduction of Thermal Conductivity by Nanoparticle Addition and Stoichiometric Change to Mg_2Si, *American Society of Thermal and Fluids Engineers Conference and 4th International Workshop on Heat Transfer*, April 2-5 2017, Las Vegas, NV, USA. *(presentation)*

- W. Tanner Yorgason and N.A. Roberts, Size Dependent Thermal Conductivity of Single-Wall Carbon Nanotubes from Molecular Dynamics Simulations, *The Minerals, Metals, and Materials Society Conference*, February 15-17 2016, Nashville, TN, USA. *(poster)*

Other Achievements

- Air Force Research Laboratory Hap Arnold Scholar

- RGS Graduate Travel Award